



TECHNISCHE
UNIVERSITÄT
WIEN

Master Thesis

**Towards continuous enantioselective
 α -alkylation of ketones *via* direct enamine
photoexcitation**

Ausgeführt am

Institut für Angewandte Synthesechemie

Unter der Leitung von

Univ. Prof. Dipl.-Ing. Dr. techn. Katharina Schröder

Eingereicht an der Technischen Universität Wien

am 03.03.2023

von

Michael Weiser, BSc



Acknowledgment

First of all, I would like to thank Prof. Katharina Schröder for granting me the opportunity to accomplish my master thesis in her research group. I am very grateful for the exciting research topic and the introduction to the intriguing field of asymmetric photocatalysis.

I would also like to thank my supervisor Ádám Pálvölgyi for giving me constructive guidance and valuable support during my work.

Also, I would like to thank the whole research group for pleasantly including me, for all the provided help and for the cheerful time during work and afterward.

Furthermore, I would like to thank everybody who supported and encouraged me during my academic career.

Last but not least, I would like to express my gratitude to my family, who incessantly supported me in all respects throughout my life, and without them, I would not have come so far.

Abstract

Motivated by the persistent difficulty of asymmetric catalytic direct intermolecular α -alkylation reactions of ketones with simple alkyl halides and their scarcity in photocatalytic processes, in this work, a new method for this synthetic task is presented.

The highly abundant and natural-derived 9-amino(9-deoxy)-*epi*-cinchona alkaloids proved to act as potent catalysts for the direct photo/organocatalytic asymmetric α -alkylation of ketones. After parameter optimization, diverse functionalized symmetric and cyclic ketones of different ring sizes could be readily reacted with symmetric electron-deficient bromomalonates and the related products could be obtained with good yield and enantioselectivity. Furthermore, this concept provided access to both enantiomeric antipodes.

Mechanistic investigations revealed the proposed reaction mechanism, which proceeds *via* a self-propagating radical chain mechanism initiated by the direct excitation of the transiently formed secondary enamine upon 365 nm irradiation.

Apart from introducing an uncomplicated procedure optimized for batch, homogeneous conditions throughout the entire reaction were found, thus enabling the photo/organocatalytic synthesis of 1,3-diethyl 2-(2-oxocyclohexyl)propanedioate in continuous-flow.

Kurzfassung

Motiviert durch die andauernde Schwierigkeit von asymmetrisch katalysierten direkten intermolekularen α -Alkylierungen von Ketonen mit einfachen Alkylhalogeniden und deren Seltenheit in photokatalytischen Prozessen wird in dieser Arbeit eine neue Methode für diese synthetische Aufgabe vorgestellt.

Die reichlich zur Verfügung stehenden und von Naturprodukten abgeleiteten 9-Amino-(9-desoxy)-*epi*-cinchona Alkaloide erwiesen sich als potente Katalysatoren für die direkte photo-/organokatalytische asymmetrische α -Alkylierung von Ketonen. Nach der Parameteroptimierung konnten divers funktionalisierte symmetrische und cyclische Ketone unterschiedlicher Ringgröße einfach mit symmetrischen elektronenarmen Brommalonaten umgesetzt und die entsprechenden Produkte mit guter Ausbeute und Enantioselektivität erhalten werden. Darüber hinaus bot dieses Konzept einen Zugang zu beiden enantiomeren Antipoden.

Mechanistische Untersuchungen führten zur Aufdeckung des vorgeschlagenen Reaktionsmechanismus, der über einen sich selbst ausbreitenden Radikalkettenmechanismus abläuft und durch die direkte Anregung des intermediär gebildeten sekundären Enamins bei 365 nm Bestrahlung initiiert wird.

Neben der Einführung eines unkomplizierten für den Batch optimierten Verfahrens wurden Bedingungen gefunden, die homogene Bedingungen während der gesamten Reaktionszeit bieten, um das photo-/organokatalytische System für die Synthese von 2-(2-Oxocyclohexyl)malonsäurediethylester im kontinuierlichen Fluss anzuwenden.

Abbreviations

AcOH	Acetic acid
Boc ₂ O	Di- <i>tert</i> -butyl decarbonate
bpy	2,2'-Bipyridine
CFL	Compact fluorescent lamp
cod	1,5-Cyclooctadiene
DBU	1,8-Diazabicyclo(5.4.0)undec-7-ene
BPR	Back pressure regulator
DCE	1,2-Dichloroethane
DCM	Dichloromethane
DEAD	Diethyl azodicarboxylate
DIPEA	<i>N,N</i> -Diisopropylethylamine
DME	Dimethoxyethane
DMF	Dimethyl formamide
DMSO	Dimethyl sulfoxide
DPPA	Diphenylphosphoryl azide
EDA	Electron donor acceptor
ee	Enantiomeric excess
Et ₂ O	Diethyl ether
EtOAc	Ethyl acetate
EWG	Electron withdrawing group
GCFID	Gas chromatography flame ionization detector
GCMS	Gas chromatography mass spectrometry
HOMO	Highest occupied molecular orbital
HOTf	Triflic acid
HPLC	High-performance liquid chromatography
HSAB	Hard and soft acids and bases
LDA	Lithium diisopropylamide

LED	Light emitting diode
LUMO	Lowest unoccupied molecular orbital
MeOH	Methanol
MOF	Metal-organic framework
MTBE	Methyl <i>tert</i> -butyl ether
NaHDS	Sodium bis(trimethylsilyl)amide
NBS	<i>N</i> -Bromosuccinimide
NEt ₃	Triethylamine
NMR	Nuclear magnetic resonance
PE	Petrol ether
PPh ₃	Triphenylphosphine
RAMP	(<i>R</i>)-1-Amino-2-methoxymethyl pyrrolidine
SAMP	(<i>S</i>)-1-Amino-2-methoxymethyl pyrrolidine
SET	Single electron transfer
SOMO	Single occupied molecular orbital
TBDMS	<i>tert</i> -Butyl-trimethylsilyl
TEMPO	2,2,6,6-Tetramethylpiperidin-1-yl)oxyl
TFA	Trifluoroacetic acid
THF	Tetrahydrofuran
TLC	Thin layer chromatography
TMS	Trimethylsilyl
UV	Ultraviolet light
Vis	Visible light
(<i>S</i>)-TRIP	(<i>S</i>)-3,3'-Bis(2,4,6-triisopropylphenyl)-1,1'-binaphthyl-2,2'-diyl hydrogenphosphate

Table of contents

1	Introduction	1
2	Basic concepts	2
2.1	Enol chemistry	2
2.1.1	α -Acidity	2
2.1.2	Keto-enol tautomerization.....	3
2.1.3	Stereochemical aspects.....	4
2.2	Catalysis	6
2.2.1	Physicochemical aspects.....	6
2.2.2	Types of catalysis	7
2.3	Photocatalysis	8
2.3.1	Definition.....	8
2.3.2	Physicochemical aspects.....	8
2.3.3	Photoredox catalysis.....	9
3	Asymmetric α-alkylation of aldehydes and ketones	11
3.1	Fundamentals	11
3.1.1	Enamine chemistry	11
3.1.2	Chiral auxiliaries	13
3.2	Catalytic methods	15
3.2.1	Transition metal catalyzed reactions	15
3.2.2	Phase-transfer catalyzed reactions	16
3.2.3	Enamine catalyzed reactions.....	17
3.2.4	Single occupied molecular orbital catalyzed reactions	19
3.3	Photocatalytic methods	21
3.3.1	Dual system strategy	21
3.3.2	Electron donor acceptor complex strategy	23
3.3.3	Direct excitation strategy	24
4	Aim of the thesis	26
5	Results and discussion	27
5.1	Reaction design	27
5.2	Condition optimization	30
5.2.1	Solvent screening	31

5.2.2	Acid and base screening	32
5.2.3	Concentration screening.....	33
5.2.4	Catalyst screening	34
5.2.5	Optimized reaction conditions.....	35
5.3	Mechanistic investigations	39
5.3.1	Control experiments.....	39
5.3.2	UV/Vis spectra	40
5.3.3	Light on/off experiment	41
5.3.4	Quantum yield.....	42
5.3.5	Proposed mechanism	43
5.4	Scope and limitation.....	45
5.4.1	Ketones.....	45
5.4.2	Alkyl halides.....	48
5.5	Continuous-flow implementation.....	50
5.5.1	Overview	50
5.5.2	Screening of conditions	50
6	Conclusion and outlook	53
7	Experimental Part	55
7.1	Materials and methods.....	55
7.2	Catalyst synthesis	57
7.2.1	(8 α ,9 <i>S</i>)-6'-Methoxycinchonan-9-amine (Qn).....	57
7.2.2	(9 <i>R</i>)-6'-Methoxycinchonan-9-amine (Qd).....	59
7.2.3	(9 <i>R</i>)-Cinchonan-9-amine (Cn)	61
7.2.4	(9 <i>S</i>)-6'-Methoxy-2'-phenylcinchonan-9-ol	63
7.2.5	(9 <i>R</i>)-6'-Methoxy-2'-phenylcinchonan-9-amine (PhQd)	64
7.2.6	(2 <i>S</i>)-1,2-Pyrrolidinedicarboxylic acid 1-ethyl 2-methyl ester.....	66
7.2.7	(2 <i>S</i>)-2-[Bis[3,5-bis(trifluoromethyl)phenyl]hydroxymethyl]-1-pyrrolidinecarboxylic acid ethyl ester	67
7.2.8	(2 <i>S</i>)- α , α -Bis[3,5-bis(trifluoromethyl)phenyl]-2-pyrrolidinemethanol	68
7.2.9	(2 <i>S</i>)-2-[Bis[3,5-bis(trifluoromethyl)phenyl][(trimethylsilyl)oxy]methyl]pyrrolidine (SA1) ..	69
7.2.10	(2 <i>S</i>)-2-[Bis[3,5-bis(trifluoromethyl)phenyl][[(1,1-dimethylethyl)dimethylsilyl]oxy]methyl] pyrrolidine (SA2).....	70
7.3	Asymmetric α-alkylation of ketones <i>via</i> direct enamine photoexcitation	71
7.3.1	Batch photoreactor set-up	71
7.3.2	Flow photoreactor set-up.....	71

7.3.3	General considerations in batch	72
7.3.4	General considerations in continuous-flow	73
7.3.5	General procedure in batch	73
7.3.6	Analytical data of α -alkylated ketones	74
7.4	Substrate synthesis.....	80
7.4.1	1,3-Dimethyl 2-bromopropanedioate (H2)	80
7.4.2	1,3-Bis(phenylmethyl) 2-bromopropanedioate (H4).....	81
7.4.3	<i>tert</i> -Butyl 4-oxopiperidine-1-carboxylate (K5)	82
7.4.4	<i>N,N</i> -Diethyl-4-oxo-1-piperidinecarboxamide (K6).....	83
7.5	Quantum yield determination.....	84
7.5.1	Synthesis of potassium ferrioxalate	84
7.5.2	Determination of the photon flux.....	85
7.5.3	Determination of the quantum yield	87
8	References.....	89

1 Introduction

As a consequence of nature's evolutionary developed specificity about controlling the configuration of asymmetric substituted C-atoms in biological monomers, chiral environments are omnipresent in biological systems. This homochirality *inter alia* enables the differentiation between enantiomers (e.g., ligands or substrates), respectively their related biological properties. Therefore, especially in modern drug synthesis, the precise control of the stereochemistry is of great importance.^{1, 2}

Several strategies have been established concerning the production of enantiopure compounds. In an industrial context, it is often convenient to take advantage of nature's chiral pool or to use well-established preparative separation techniques of the enantiomers of a racemate (*via* crystallization, kinetic resolution, diastereomeric resolution or chiral chromatography). However, the most elegant strategy for producing enantiopure or enantioenriched compounds is asymmetric synthesis and therefore, the selective introduction of the desired stereochemical information.³

In green chemistry, asymmetric synthesis is advantageous over racemic separation methods since the latter maximally yields half of the racemic product as the desired enantiomer (unless combined with *in situ* racemization) and thus produces less waste.³ In the last decade, significant effort has been taken into developing photocatalytic methods that utilize visible light instead of thermal energy as an energy source. The renewable and pollution-free harvest of energy in the form of photons provided by the sun and its storage in chemical bonds meets the demand for sustainability in chemistry.⁴

Therefore, the development of photocatalytic methods, primarily to target the construction of valuable fine chemicals with attention to asymmetric synthesis offers excellent potential to aim for modern needs.

2 Basic concepts

2.1 Enol chemistry

2.1.1 α -Acidity

The carbonyl group is one of the most widespread functional groups among biomolecules and therefore, undoubtedly of particular importance in organic synthesis. The C=O double bond in aldehydes and ketones offers a broad versatility of possible chemical manipulations, e.g., oxidation, reduction and condensation, due to the electrophilic behavior of the positive polarized C-atom and the lone pairs of the negative polarized O-atom. Aside from chemical reactions that take place directly at the carbonyl group, alkyl substituted aldehydes and ketones (and other related structures with π -electron withdrawing groups and without more acidic H-atoms, e.g., esters, nitriles or *N,N*-disubstituted amides) offer another site of reactivity. As a consequence of the π -electron withdrawing behavior of the carbonyl group, C-H bonds adjacent to the carbonyl group show a certain acidity, as the conjugated base – the enolate ion – is well resonance stabilized. The members of these acidic C-H bonds are called α -C or α -H atoms, and the underlying reactivity is called α -acidity. In organic synthesis, the α -acidity of carbonyl species is exploited to establish nucleophilic reactivity at the α -C atom and thus to enable the reaction with electrophiles, most frequently to attach an alkyl group at the α -C atom. The α -alkylation is one of the most important C-C bond-forming reactions. α -Alkylation reactions can be divided into those that rely on the nucleophilic addition to C=O (e.g., Aldol), C=N (e.g., Mannich) or C=C (e.g., Michael) double bonds, and those that rely on nucleophilic substitution reactions (Figure 1).⁵

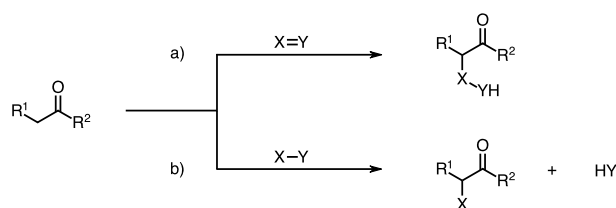


Figure 1: α -Alkylation of an aldehyde ($R^2 = H$) or a ketone ($R^2 = \text{alkyl}$) via nucleophilic addition (a) or nucleophilic substitution (b).⁵

2.1.2 Keto-enol tautomerization

In a solution of aldehydes or ketones, the carbonyl species exist in equilibrium with their tautomeric enol species. In general, the carbonyl species is dominant over the enol species. Still, the equilibrium position is particularly influenced by the solvent and whether other stabilizing effects, e.g., aromatization, are present. The formation of the enol species can be accelerated through acid or base catalysis. In the presence of an acidic catalyst, the basic carbonyl O-atom of the carbonyl species is protonated, enhancing the acidity of the α -C-H bond. The enol species is formed after deprotonation of the acidic α -H atom and equalization of the positive charge (Figure 2a). A basic catalyst abstracts an acidic α -H atom of the carbonyl species, forming an enolate ion, which is resonance stabilized by the π -system of the carbonyl bond. The negative charge is dominantly located on the more electronegative O-atom. In accordance with the HSAB concept, the hard, negatively charged O-atom abstracts a proton, forming the enol species (Figure 2b).^{5, 6}

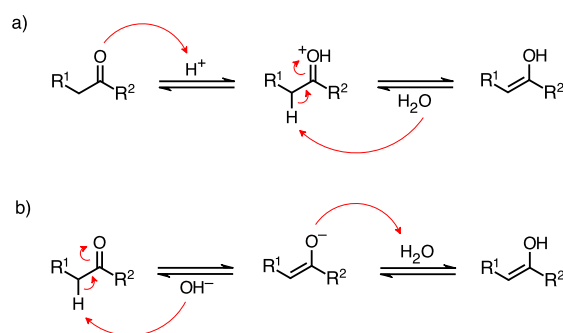


Figure 2: Acid (a) and base (b) catalyzed keto-enol tautomerization of an aldehyde ($R^2 = H$) or a ketone ($R^2 = \text{alkyl}$).⁵

Compared to alkenes, the C=C double bond of enols is substituted with an electronegative O-atom, whose lone pairs can participate in the C=C π -system. Consequently, the HOMO is energetically enhanced. Therefore, enols are better nucleophiles than alkenes. Since the largest orbital coefficient of the HOMO is located at the α -C atom, the soft center is located there. Therefore, nucleophilic reactions will dominantly take place at the α -C atom.⁶

2.1.3 Stereochemical aspects

Aldehydes and ketones with two different substituents bound to the α -C atom – apart from the acidic α -H atom – undergo α -alkylation reactions with the formation of an asymmetric substituted α -C atom, respectively, two enantiomers can be formed. If no stereocontrol is provided, both enantiomers are formed equally, whereas otherwise, a racemic product is obtained. Non-symmetric alkyl substituted ketones if both alkyl substituents of the carbonyl group exhibit acidic α -H atoms, offer two possible sites for enolization, respectively, where an α -alkylation reaction can take place. Therefore, regio- and stereochemical aspects must be controlled, especially for ketones, to ensure the selective formation of one defined enantiomer. As a consequence of the sp^2 -hybridization of the C=C double bond of an enol and its planar geometry, enols offer two sites from where an electrophilic attack can happen (Figure 3b). In dependence on the substituents bound to the α -C atom, the facial sites of an enol can be homotopic, enantiotopic or diastereotopic. If the α -C atom is substituted equally, the facial sites are homotopic, and an α -alkylation reaction will lead to one defined product. If the α -C atom is substituted differently, the facial sites are enantiotopic. An α -alkylation reaction will lead to the formation of enantiomers that differ in the α -C atom configuration. If there is already chirality in the molecule and the α -C atom is substituted differently, the facial sites are diastereotopic. In that case, an α -alkylation reaction will lead to the formation of diastereomers. Apart from that, if the α -C atom of the enol is differently substituted, two geometric isomers can be distinguished. Whether the α -C atom substituent with the higher priority is located on the same side or the other side of the double bond as the former carbonyl O-atom, the terms *Z* or *E* are used (Figure 3a).^{5, 7}

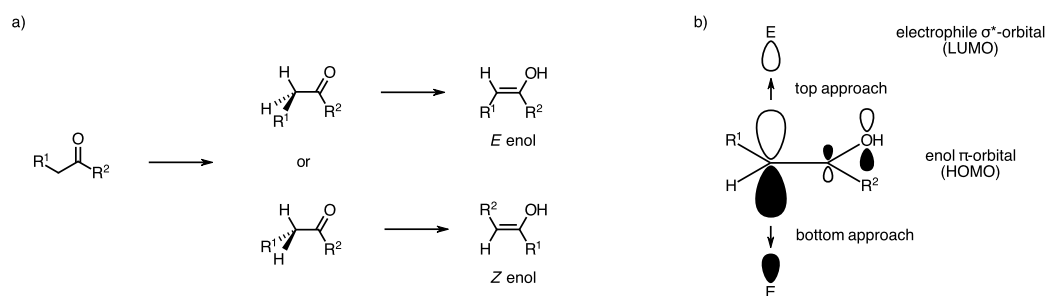


Figure 3: Discrimination between geometrical isomers (a) and between facial sites (b) of enols.⁷

The selective formation of one defined α -C atom constitution can be achieved by controlling the formation of one geometric isomer and selecting one enantiotopic (or diastereotopic) facial site for the electrophilic attack.⁷

2.2 Catalysis

2.2.1 Physicochemical aspects

In general, the outcome of a chemical reaction is defined by thermodynamic and kinetic aspects. The substrates (A + B) and the products (P) are assigned to a certain free enthalpy (G^0), and the free reaction enthalpy (ΔG^0) is related to the equilibrium constant (Figure 4). A chemical reaction can only take place if its exergonic, respectively the reaction enthalpy is negative. Therefore, the thermodynamic rules about the position of the equilibrium. On the other hand, within a chemical reaction bonds must be broken and new bonds must be formed, whose transition state ($\{A \cdot B\}^\#$) is assigned to a free activation enthalpy ($\Delta G^{0\#}$) that defines the activation barrier. The height of the activation barrier is related to the rate at which the equilibrium is reached. The required energy to overcome the activation barrier is classically provided by thermal energy. The use of a catalyst changes the reaction mechanism and accelerates the equilibrium adjustment by providing lower energy ($\Delta G_K^{0\#}$) transition states ($\{A \cdot K \cdot B\}^\#$).⁸

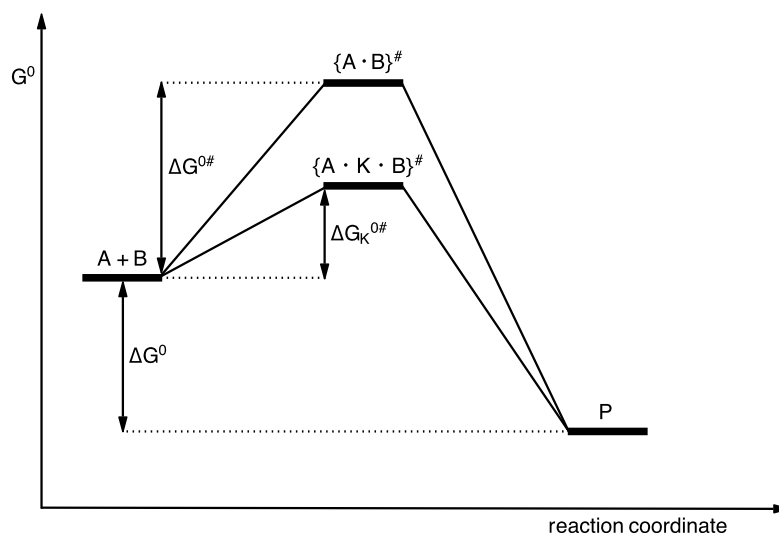


Figure 4: Impact of a catalyst on the free enthalpy of a chemical reaction.⁸

Thermodynamic aspects of the chemical reaction and thus, the equilibrium position are not changed by using a catalyst. The selectivity of a catalyst towards a certain chemical reaction is based on the acceleration of the underlying reaction pathway.⁸

2.2.2 Types of catalysis

The broad field of catalysis can be generally divided into homogeneous and heterogeneous catalysis. A homogeneous catalyst is located in the same phase as the reagents and a heterogeneous catalyst is located in a different phase than the reagents. Since many heterogeneous catalyzed reactions involve a solid inorganic catalyst and gaseous or liquid reagents, they are related to advantages like uncomplicated separation and processing and high thermal and chemical stability. Contrarily, homogeneous catalysts typically benefit from high selectivity and activity due to their molecular nature. By another classification of catalytic processes, biocatalysis, (transition-) metal catalysis and organocatalysis can be distinguished.^{3, 9}

Organocatalysis offers a broad versatility of conceptually different substrate activations. It can be further divided into amino catalysis (enamine and iminium catalysis), H-bond catalysis, phase-transfer catalysis, counter-ion catalysis and *N*-heterocyclic carbene catalysis. By that meaning, the activation can originate from forming a covalent bond (amino catalysis and *N*-heterocyclic carbene catalysis) or from non-covalent interactions (phase transfer catalysis, counter-ion catalysis, H-bond catalysis) between the substrate and the catalyst (Figure 5).¹⁰

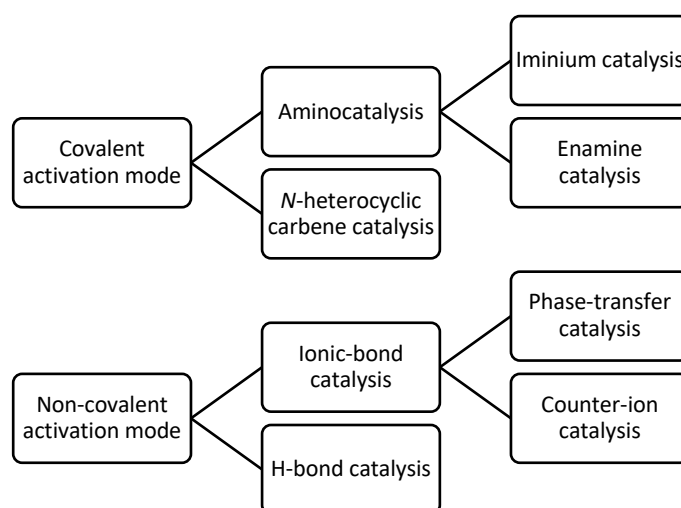


Figure 5: Overview of classic organocatalytic processes.¹⁰

2.3 Photocatalysis

2.3.1 Definition

Inspired by nature's photosynthesis, the utilization of photons ($h\nu$) by a photocatalyst, respectively, the utilization of its energy instead of thermal energy to facilitate chemical reactions define the field of photocatalysis. The participation of photons as a reagent harvested by a photocatalyst can enable chemical reactions that are referred to as thermodynamically impossible under thermal conditions or can enhance hindered kinetics of spontaneous chemical reactions. As for the definition of classic catalysis, photocatalysis can be divided into homogeneous and heterogeneous photocatalysis with the respective characteristics. While heterogeneous photocatalysis is based on inorganic semiconductors, molecular solutions of organic dyes or transition metal-based complexes refer to homogeneous photocatalysis.⁴

2.3.2 Physicochemical aspects

The initial step of a homogeneous photocatalytic reaction is the absorption of light, where an electron is promoted from an occupied orbital, typically the HOMO, into an empty orbital, typically the LUMO. As a consequence of the antibonding character and the single electron population of the LUMO or higher energy orbitals, the geometry and electronic structure of the excited state alters from the ground state, thus justifying its enhanced reactivity.^{11, 12}

In a more detailed point of view (Figure 6), upon absorption (A), the electronic singlet ground state (S_0) turns into the first electronic singlet excited state (S_1). Depending on the excess energy provided by the irradiation, several vibrational (and rotational) states (V) are excited. These excited states within S_1 readily relax to the vibrational ground state of S_1 under emission of thermal energy. Subsequently, S_0 recovers from this energy level *via* radiative (emission of $h\nu$; fluorescence, F) or non-radiative (emission of thermal energy; internal conversion, IC and vibrational relaxation, VR) pathways. Intersystem crossing (ISC) describes the spin-forbidden transition from S_1 to excited vibrational (and rotational) states of the first electronic triplet state (T_1). After vibrational relaxation to the vibrational ground state of T_1 , relaxation to S_0 can occur

via radiative (emission of $h\nu$; phosphorescence, P) or non-radiative (emission of heat; ISC and VR) pathways, which both are spin-forbidden.¹³

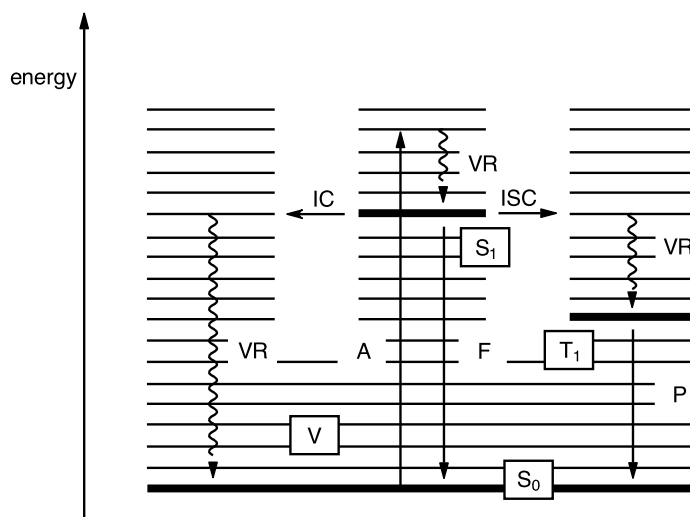


Figure 6: Jablonski term schema.¹³

Both types of excited states (S_1 and T_1) are feasible to engage chemical reactions with a typically bimolecular nature. Since the excited state photocatalyst and the reactant must encounter *via* diffusion to react, the excited state lifetime must be sufficiently long. As a consequence of the spin-forbidden decay, T_1 (μs to ms) is more persistent than S_1 (ns). Therefore, it is more likely to participate in chemical reactions. On the other hand, S_1 features a more powerful redox reactivity than T_1 as a consequence of its higher energy.¹³

2.3.3 Photoredox catalysis

Within a photo catalyzed reaction, the photocatalyst's excited state (S_1 or T_1) is quenched by a reactant, thus producing reactive species *via* photo-induced atom (or group), energy or electron transfer processes. The latter reactivity is referred to as photoredox catalysis and can pursue *via* two possible quenching cycles (Figure 7). In the oxidative cycle, the excited state of the photoredox catalyst (cat^*) is quenched by donating an electron to an acceptor (A) that is subsequently reduced (A^-). The

remaining oxidized photoredox catalyst (cat^+) accepts an electron from a donor (D), which is subsequently oxidized (D^+) so that the ground state of the photoredox catalyst (cat) is recovered. In the reductive cycle, the excited state of the photoredox catalyst (cat^*) is quenched by accepting an electron from a donor (D) that is subsequently oxidized (D^+). The remaining reduced photoredox catalyst (cat^-) donates an electron to an acceptor (A), which is subsequently reduced (A^-) so that the ground state of the photoredox catalyst (cat) is recovered.¹¹⁻¹³

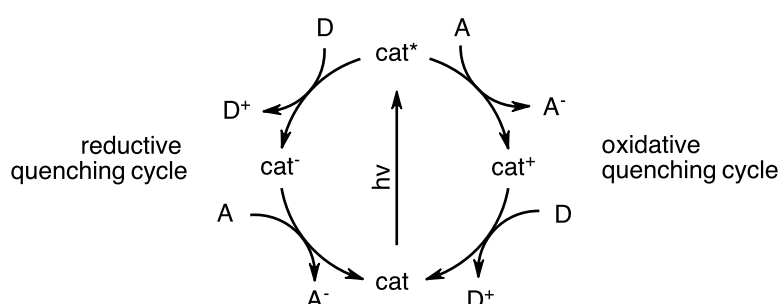


Figure 7: Reductive and oxidative quenching cycle of photoredox catalysis.¹³

From a thermodynamical perspective, it is noteworthy that the redox potential of the excited state of the photoredox catalyst ($E(\text{cat}^+/\text{cat}^*)$) or of the reduced photoredox catalyst ($E(\text{cat}/\text{cat}^-)$) must be more negative than the redox potential of the acceptor ($E(\text{A}/\text{A}^-)$) in order to reduce it. Contrarily, the redox potential of the excited state of the photoredox catalyst ($E(\text{cat}^*/\text{cat}^-)$) or of the oxidized photoredox catalyst ($E(\text{cat}^+/\text{cat})$) must be more positive than the redox potential of the donor ($E(\text{D}^+/\text{D})$) in order to oxidize it.¹³

3 Asymmetric α -alkylation of aldehydes and ketones

3.1 Fundamentals

Mimicking enzymes, which are biocatalysts that nature has optimized for specific synthetic applications and that are highly selective, is one of the most significant challenges in organic synthesis. While the enzymatic stereoselectivity is explained by the three-attachment model and the elevated acceleration of the production of the favored enantiomer is based on an elevated transition state stabilization, the energetically favored pathway and thus, the stereodiscrimination of an artificial asymmetric catalyst is primarily explained by steric effects.^{2, 14}

3.1.1 Enamine chemistry

The nucleophilic behavior of especially enolates can be used for α -alkylation reactions *via* a nucleophilic substitution mechanism. Despite its ease, this technique suffers from many side reactions, e.g., polyalkylation, self-aldolization, competing O- and C-alkylation and many more. However, using bases that provide a large counterion (e.g., K^+) for the enolate-ion facilitates C-alkylation since the negatively charged O-atom is sterically blocked. The reduced reactivity of metal enolates of less electropositive elements, e.g., silyl enol ether, prevents self-aldolization since they only react with activated alkyl halides. Seminal work by Stork *et al.* established preformed enamines as a surrogate to enolates to prevent polyalkylation. Additionally, sterically hindered amines can be used for enamine formation in order to avoid *N*-alkylation side reactions.¹⁵

Enamines can thus be considered analogs to enols. As a consequence of the participation of the electronegative lone pairs of the N-atom in the C=C π -system, an energetically elevated HOMO and thus, an enhanced nucleophilicity is observed. Since the largest coefficient of the HOMO is located at the α -C atom, it is most likely to react as a nucleophile with electrophiles, according to the HSAB concept.⁶ Apart from that, the same considerations concerning stereocontrol made for enols are valid for enamines.

Enamines are typically prepared by acid catalyzed condensation of an aldehyde or ketone with an amine, resulting in the removal of one water molecule (Figure 8). Since the reaction is reversible, water must be continuously removed to shift the equilibrium towards the product for a quantitative formation of the condensation product. In the first step, the amine adds to the C=O double bond under the formation of a hemiaminal. After protonation of the hydroxy group to form a better leaving group, it is eliminated by the lone pair of the N-atom under the formation of an iminium ion. If a secondary amine is used and α -H atoms are available, an enamine is formed, while the reaction stops at the iminium ion stage in the absence of α -H atoms. A primary amine forms an imine that exists in equilibrium with an enamine in dependence if α -H atoms are available.^{5, 16}

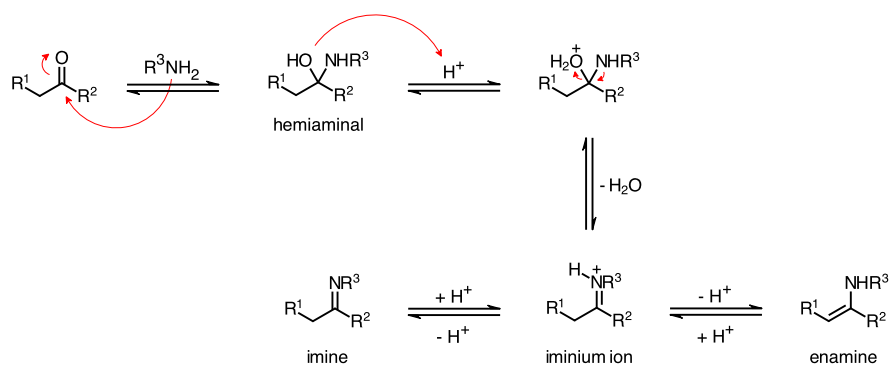


Figure 8: Condensation of a primary amine with an aldehyde ($R^2 = \text{H}$) or a ketone ($R^2 = \text{alkyl}$).⁵

As a consequence of the reversibility of the condensation, enamines, imines and iminium ions can be hydrolyzed to recover the respective aldehyde or ketone. This behavior, accompanied by substrate activation and stereoinduction, renders chiral amines as potent asymmetric catalysts, thus establishing the field of asymmetric amino catalysis. Concerning enamine catalysis, various primary and secondary chiral amines are known to enable α -alkylation reactions of aldehydes and ketones with high diastereoselectivity.^{17, 18}

3.1.2 Chiral auxiliaries

The classic strategy for the asymmetric α -alkylation of aldehydes and ketones is the stoichiometric use of chiral auxiliaries. As a consequence of their robustness and reliability but multiple step procedure and low atom economy, they are most frequently applied in target-directed synthesis. The covalent attachment of a chiral auxiliary to the carbonyl species, followed by the deprotonation of the α -H-atom, yields an intermediate with a planar C=C double bond and diastereotopic sites. Geometric isomer formation and preferential site of attack are dictated by steric repulsions.^{19, 20}

The most frequently used chiral auxiliaries applicable for aldehydes and ketones are Ender's SAMP and RAMP, which provide access to both enantiomeric antipodes (Figure 9).

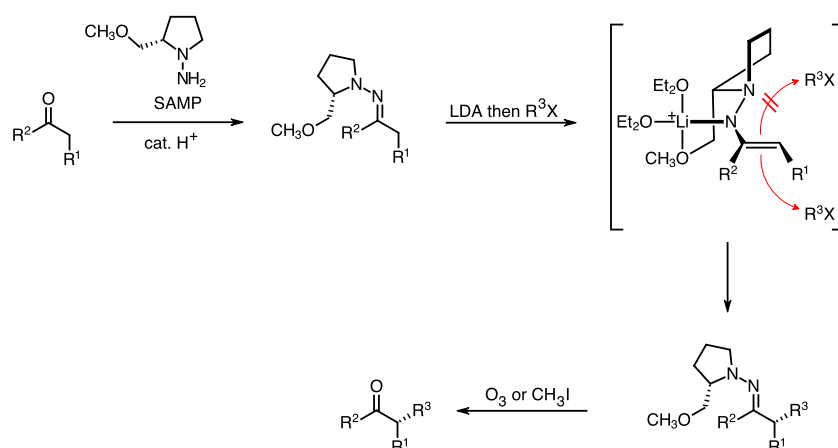


Figure 9: Asymmetric α -alkylation of an aldehyde ($R^2 = H$) or a ketone ($R^2 = \text{alkyl}$) using Ender's SAMP.²⁰

The four-step synthesis covers the steps of attachment of the chiral auxiliary, α -H deprotonation, α -alkylation and cleavage of the chiral auxiliary. In an analogous mechanism to the imine formation, a hydrazine condenses with an aldehyde or ketone under the formation of a hydrazone. The α -H deprotonation of the hydrazone with lithium bases like LDA yields the formation of an aza enolate that exists in a six-membered chelate. It has been shown that although four geometrical isomers can be theoretically distinguished, only the $E_{CC}Z_{CN}$ species is formed. As a consequence of the steric shielding of one diastereotopic site of the aza enolate, the electrophilic attack occurs

highly diastereoselective. To preserve the stereochemical information, the hydrazone must be cleaved under mild conditions, thus obtaining the enantioenriched α -alkylated aldehyde or ketone by ozonolysis or reaction of the hydrazone with methyl iodide.^{20, 21}

3.2 Catalytic methods

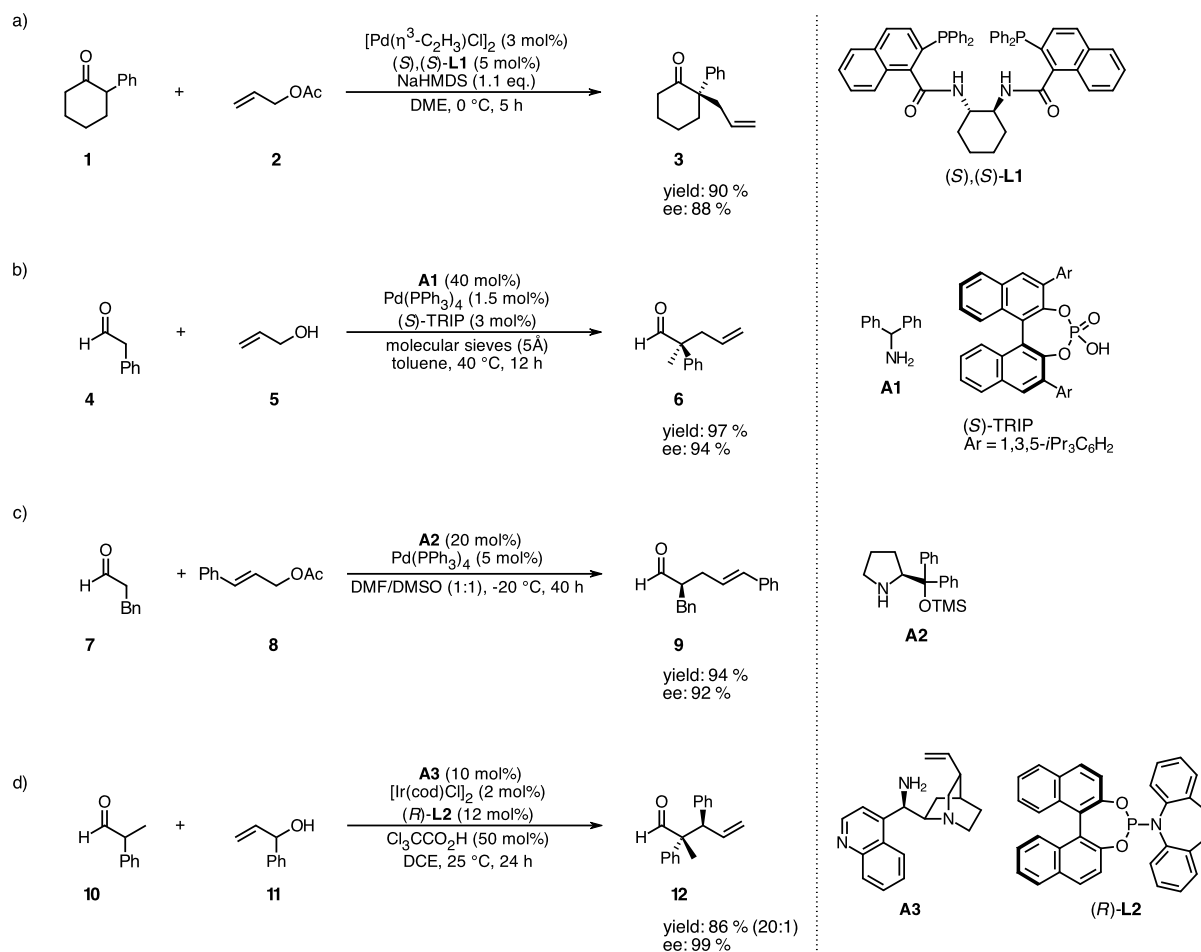
The more efficient and sustainable method to target the asymmetric α -alkylation of carbonyl species is selective asymmetric catalysts rather than using stoichiometric chiral auxiliaries. Additionally, direct methods are of particular interest to reduce additional reaction steps and thus reduce waste generation. They differentiate from indirect methods, as they transiently form the activated species by interacting with the catalyst rather than relying on a preformed activated species, e.g., Lewis acid activated carbonyl species interacting with the catalyst.²²

In the following section, asymmetric catalyzed direct α -alkylation reactions of aldehydes and ketones with important contributions to the field will be briefly presented.

3.2.1 Transition metal catalyzed reactions

Within transition metal catalysis, the Tsuji-Trost reaction represents a versatile method for the direct asymmetric α -allylation of aldehydes and ketones. In 2002 Trost *et al.*²³ (Scheme 1a) reported the base-assisted asymmetric α -allylation of 2-phenylcyclohexanone **1** with allyl acetate **2** via transition metal catalysis using a chiral ligand ((*S*),(*S*)-**L1**) to afford the α -allylated product **3**. The prevention of stoichiometric base for the enolate nucleophile formation and thus, the reduction of produced waste was achieved by the execution of the Tsuji-Trost reaction with an enamine co-catalyst. In 2011 List *et al.*²⁴ (Scheme 1b) reported the α -allylation of an aldehyde **4** via a combination of transition metal, enamine and counter-ion catalysis. The enamine transiently formed by condensation of **4** with the primary amino catalyst (**A1**) readily attacks the cationic π -allyl Pd complex of the allyl alcohol **5** under the formation of the α -allylated product **6**, thereby directing the stereochemical outcome with a chiral phosphoric acid ((*S*)-TRIP). In 2012 Córdova *et al.*²⁵ (Scheme 1c) reported the α -allylation of an aldehyde **7** with an allyl acetate **8** via a combination of transition metal and enamine catalysis to afford the α -allylated product **9**, with enantioselectivity induced by the use of a chiral secondary amino catalyst (**A2**). In 2013 Carreira *et al.*²⁶ (Scheme 1d) reported the α -allylation of an aldehyde **10** with an allyl alcohol **11** via a combination of transition metal and enamine catalysis using a chiral ligand ((*R*)-**L2**) and a chiral primary amino

catalyst (**A3**). Apart from the depicted α -allylated product **12**, the other three stereoisomers were accessible by other amino catalyst and ligand combinations (not shown).²⁷

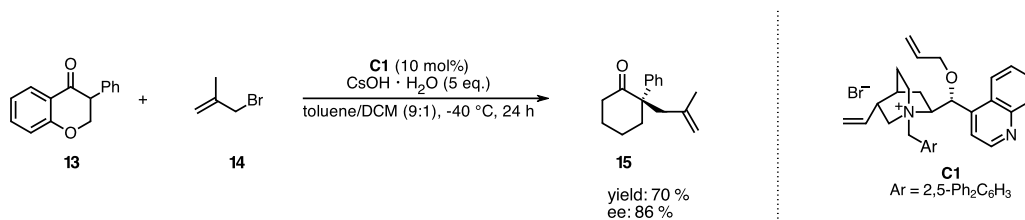


Scheme 1: Examples for direct asymmetric transition metal catalyzed α -allylation reactions.²³⁻²⁶

3.2.2 Phase-transfer catalyzed reactions

Phase-transfer catalysis is also a potent method for the direct asymmetric α -alkylation of aldehydes and ketones under biphasic conditions. Typically, a water-soluble inorganic hydroxide or alkoxide base is transferred into the organic phase, where it deprotonates the carbonyl species under the formation of an enolate. As a result of close electrostatic interactions with the chiral phase-transfer catalyst, the enolate can react asymmetrically with the alkylating agent. In 2009 Scheidt *et al.*²⁸ (Scheme 2) reported

the direct asymmetric α -alkylation of isoflavone **13** with an allyl bromide **14** under the formation of the α -allylated product **15** using a cinchona alkaloid derived phase-transfer catalyst (**C1**). Since concurrent side reactions, especially aldol additions, occur under basic conditions, the method is limited to active alkyl halides (allyl, benzyl and propargyl halides).¹⁵

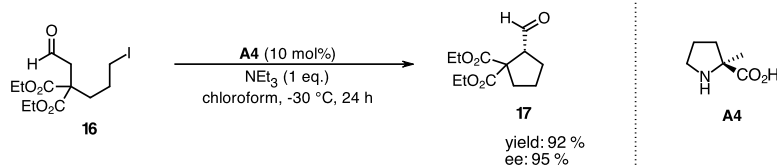


Scheme 2: Example of a direct asymmetric phase-transfer catalyzed α -allylation reaction.²⁸

3.2.3 Enamine catalyzed reactions

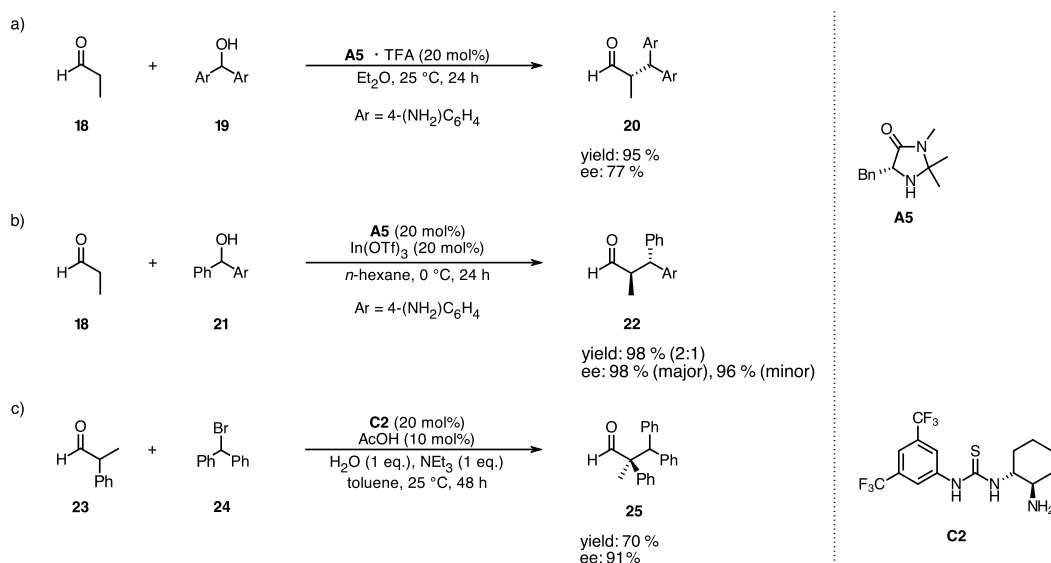
Despite considerable advances in direct asymmetric α -alkylation of aldehydes and ketones *via* enamine catalysis that undergo nucleophilic additions to C=O (Aldol), C=N (Mannich) and C=C (Michael) double bonds, those that undergo nucleophilic substitutions remain a challenging problem. The main reasons for this are the previously mentioned numerous side reactions. Furthermore, the competitive enolization, which leads to epimerization and the loss of the newly installed stereochemical information of tertiary asymmetric substituted α -C atoms, restricts the success. As a consequence of the limited nucleophilicity of enamines, their suitability for electrophiles is restricted, wherefore particularly intramolecular S_N2, intermolecular S_N1 reactions and dual catalyzed systems are known.^{15, 17, 19}

In 2004 List²⁹ *et al.* (Scheme 3) reported the direct intramolecular asymmetric α -alkylation of a halide-functionalized aldehyde **16** under the formation of the cyclic α -alkylated product **17** *via* an enamine catalyzed S_N2 mechanism using a chiral secondary amino catalyst (**A4**).



Scheme 3: Example of a direct asymmetric enamine catalyzed α -alkylation reaction *via* an intramolecular S_N2 mechanism.²⁹

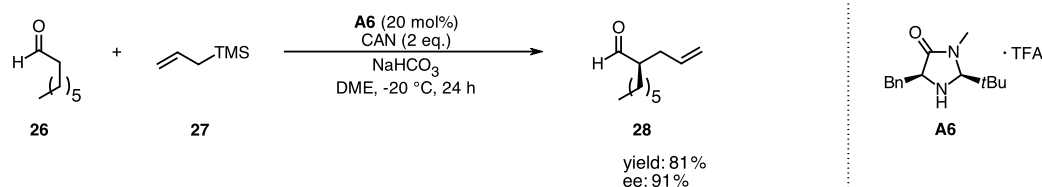
In 2009 Cozzi *et al.*³⁰ (Scheme 4a) reported the direct intermolecular asymmetric α -alkylation of an aldehyde **18** with an alcohol **19** that readily forms a stable carbocation under acidic conditions. The carbocation is subsequently intercepted *via* an enamine catalyzed S_N1 mechanism to afford the α -alkylated product **20** using a chiral secondary amino catalyst (**A5**). In 2012 Cozzi *et al.*³¹ (Scheme 4b) showed a similar Lewis acid co-catalyzed method that made an alcohol **21** accessible that cannot be activated as a carbocation *via* Brønsted acid catalysis to form the α -alkylated product **22**. In 2010 Jacobsen *et al.*³² (Scheme 4c) reported the direct intermolecular asymmetric α -alkylation of an aldehyde **23** with an alkyl halide **24** that forms a stable carbocation upon halide abstraction *via* H-bond catalysis. The transiently formed enamine subsequently intercepts the carbocation *via* an S_N1 mechanism to afford the α -alkylated product **25** using a dual enamine/H-bond catalyst (**C2**).¹⁵



Scheme 4: Examples for direct asymmetric enamine catalyzed α -alkylation reactions *via* an intermolecular S_N1 mechanism.³⁰⁻³²

3.2.4 Single occupied molecular orbital catalyzed reactions

In contrast to the previously discussed catalytic methods that are based on ionic reactions of closed shell molecules, MacMillan *et al.*³³ (Scheme 5) reported the revolutionary concept of SOMO catalysis in 2007.



Scheme 5: Example of a direct asymmetric SOMO catalyzed α -allylation reaction.³³

This radical-based activation method represents a special type of enamine catalysis that particularly facilitates the direct asymmetric α -alkylation of aldehydes and ketones. This predetermined application can be explained by its orthogonal nature compared to ionic methods and the circumvention of previously mentioned side reactions like self-aldolization. Suitable amino catalysts for SOMO catalysis are limited by the necessity for the selective oxidation of the transiently formed enamine in the presence of the amino catalyst, carbonyl species and intermediately formed iminium ion. Also, the alkylation agent must provide suitable redox properties from a thermodynamic perspective. Mechanistically (Figure 10), the transient enamine formed by condensation of an aldehyde **26** (or ketone) with a chiral secondary amino catalyst (**A6**) is oxidized by a SET agent – typically CAN. Removing an electron from the HOMO leaves behind a SOMO whose remaining energy and largest orbital coefficient at the α -C atom causes the formation of an electrophilic radical cation that is most likely to react at the α -C atom.⁶ Therefore, a nucleophilic somophile with an electron-rich π -system is readily intercepted. Among the broad versatility of SOMO catalysis, in the case of α -allylation reactions, an allylic silane **27** is classically used. Upon further oxidation by a SET agent and β -elimination of the silyl cation, an iminium ion is intermediately formed and subsequently hydrolyzed, releasing the α -allylated product **28**. Despite its

revolutionary potential concerning asymmetric α -alkylation of aldehydes and ketones, the decisive drawback of SOMO catalysis is its need for two equivalents of SET agent.³⁴

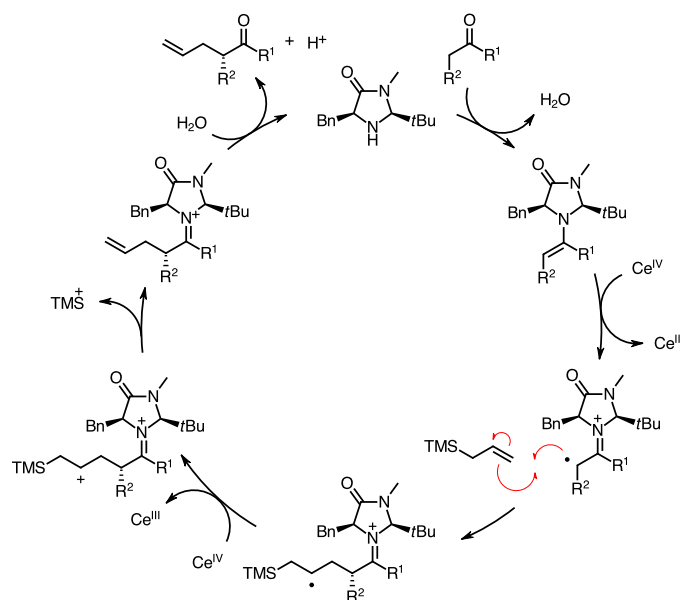


Figure 10: Mechanism of SOMO catalysis for the α -allylation of an aldehyde ($R^1 = H$) or a ketone ($R^1 = alkyl$) with allylic silanes.³⁴

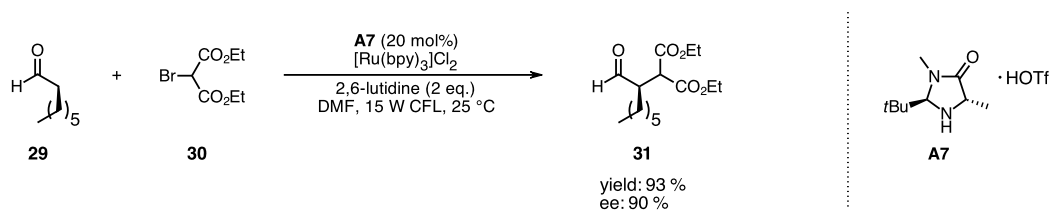
3.3 Photocatalytic methods

Photocatalytic methods continued the new acquisition of open-shelled reactivity established by SOMO catalysis. Excited-state chemistry facilitates various types of unique reactivities and chemical transformations that would not be feasible under classic ground-state conditions, e.g., the generation of highly reactive radical species under mild conditions. Owing to remarkable progress within the past few years, the application of photocatalysis in asymmetric synthesis was achieved by various stereodiscriminating methods, primarily relying on asymmetric organocatalysis.^{11, 35}

Three main strategies have been investigated concerning the direct photocatalytic asymmetric α -alkylation of aldehydes (and ketones) *via* an enamine co-catalyst, dual catalyzed systems, EDA complexes and direct excitation.¹¹

3.3.1 Dual system strategy

In 2008 MacMillan *et al.*³⁶ (Scheme 6) reported the direct asymmetric α -alkylation of aldehydes with electron-deficient alkyl halides *via* a synergistic combination of photoredox and enamine catalysis.



Scheme 6: Example of a direct asymmetric dual enamine/photoredox catalyzed α -alkylation reaction.³⁶

This overall redox-neutral dual catalyzed system founded the field of asymmetric photocatalysis. Mechanistically, the transient enamine formed by condensation of an aldehyde **29** with a chiral secondary amino catalyst (**A7**) asymmetrically intercepts the alkyl radical formed *via* reductive cleavage of an alkyl halide **30** within the reductive quenching cycle of the photoredox catalyst (Figure 11). The formed α -amino radical species is oxidized to an iminium ion by the excited photoredox catalyst that releases

the α -alkylated aldehyde **31** upon hydrolysis. In contrast to SOMO catalysis, no formal umpolung occurs since no oxidation of the nucleophilic enamine proceeds. Therefore, an electrophilic radical can be intercepted.³⁵

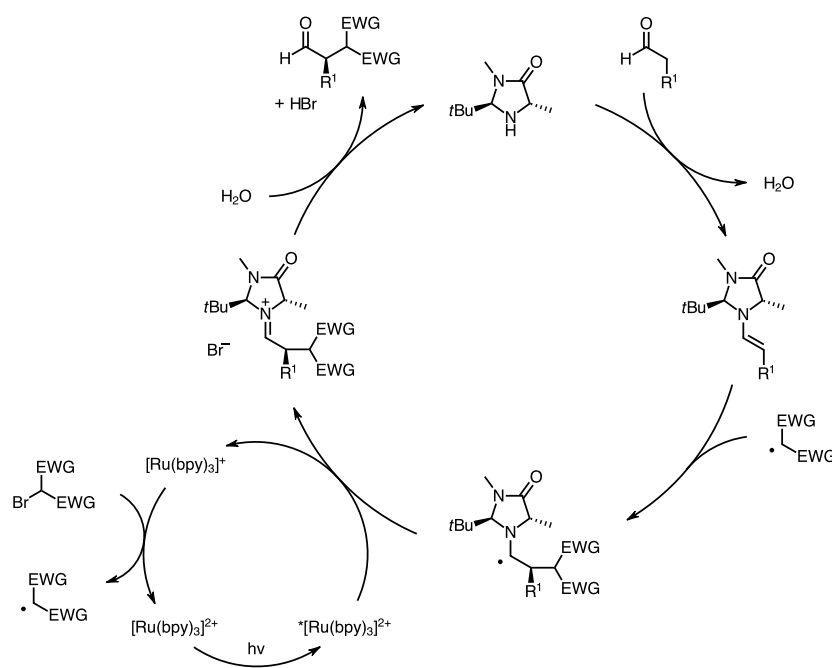
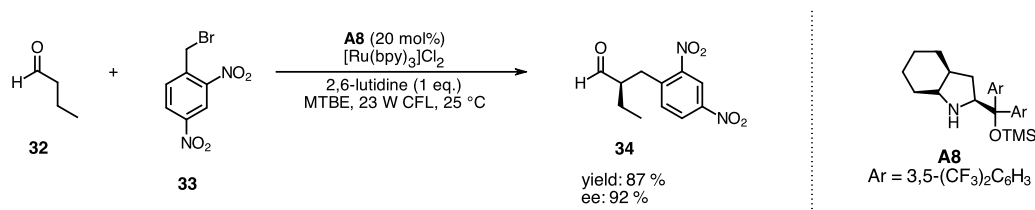


Figure 11: Mechanism of dual enamine/photoredox catalysis.³⁶

Among all photoredox catalysts, $[Ru(bpy)_3]^{2+}$ is most frequently used as a consequence of its efficient and selective excitation, sufficiently long excited state lifetime and potent redox properties.¹² The concerns accompanied with transition metal catalysts, e.g., scarcity caused expense and detrimental traces within the product, encouraged the development of metal-free alternatives of dual catalyzed systems that rely on organic dyes as a photoredox catalyst.³⁷ Also, heterogeneous photoredox systems have been developed to address separation difficulties, e.g., based on MOFs.³⁸ In the following years, several similar dual catalyzed methods for implementing different electron-deficient α -alkyl substituted aldehydes and ketones (1,3-diketones)³⁹ have been developed.¹¹

3.3.2 Electron donor acceptor complex strategy

In 2013 Melchiorre *et al.*⁴⁰ (Scheme 7) investigated light-absorbing chiral EDA complexes of transiently formed enamines and electron-deficient alkyl halides as a powerful platform for the photoredox catalyst-free photocatalytic asymmetric α -alkylation of aldehydes.



Scheme 7: Example of a direct asymmetric enamine/photo catalyzed α -alkylation reaction via EDA complex formation.⁴⁰

An EDA complex is a molecular aggregate of an electron donor, represented by the π -electron rich enamine and an electron acceptor, represented by the π -electron-deficient alkyl halide. As a consequence of the EDA complex formation, the absorption behavior changes in contrast to the separated compounds and is shifted towards higher wavelengths, allowing a selective excitation of the EDA complex. Within an excited EDA complex a charge-transfer event takes place, which is expressed by a SET – an oxidation of the electron donor and a reduction of the electron acceptor. To avoid a back electron transfer, electron acceptors with a leaving group are exploited, particularly electron-deficient alkyl halides that trap the radical species through reductive cleavage of the halide. Mechanistically, an inner-complex recombination and an outer-complex radical chain reaction can be distinguished (Figure 12). It has been shown that the former mechanism is prior. The transient enamine formed by condensing an aldehyde **32** with a chiral secondary amino catalyst (**A8**) forms an EDA complex with an alkyl halide **33**, which upon subsequent excitation, forms a radical ion pair. After the reductive cleavage of the halide, the alkyl radical asymmetrically recombines with the radical cation. The thereby formed iminium ion hydrolytically releases the α -alkylated product **34**. Among many other synthetic applications of EDA complexes,

Melchiorre *et al.*⁴¹ reported in 2014 the photocatalytic asymmetric α -alkylation of ketones with electron-deficient alkyl halides and chiral primary amino catalysts.^{11, 42}

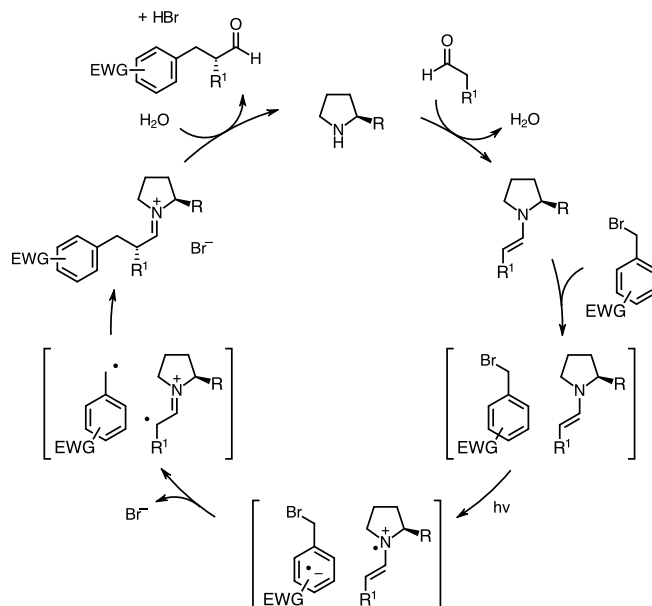
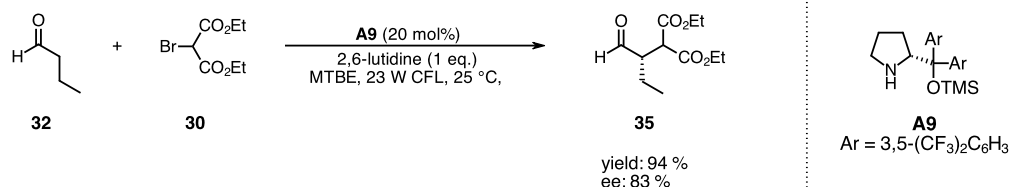


Figure 12: Mechanism of enamine/photocatalysis *via* EDA complex formation.⁴⁰

3.3.3 Direct excitation strategy

In 2015 Melchiorre *et al.*⁴³ (Scheme 8) further reported the light-induced direct asymmetric α -alkylation of aldehydes with electron-deficient alkyl halides and a chiral enamine catalyst *via* direct enamine excitation.



Scheme 8: Example of a direct asymmetric enamine/photo catalyzed α -alkylation reaction *via* direct excitation.⁴³

As no external photoredox catalyst was used and the formation of an EDA complex was ruled out, the authors suggested that the transiently formed chiral enamine acted

as a photoinitiator and initiated a radical chain reaction. Mechanistically, a small part of the excited state of the transient enamine formed by condensation of an aldehyde **32** with a chiral secondary amino catalyst (**A9**) is quenched by an alkyl halide **30** to yield a radical ion pair (Figure 13). Subsequently, after the reductive cleavage of the alkyl halide, the alkyl radical is asymmetrically intercepted by the ground-state enamine. The formed α -amino alkyl radical triggers the reductive cleavage of the alkyl halide to form an iminium ion that hydrolytically releases the α -alkylated product **35**. The newly formed alkyl radical propagates the radical chain reaction by being intercepted by the ground-state enamine.⁴³

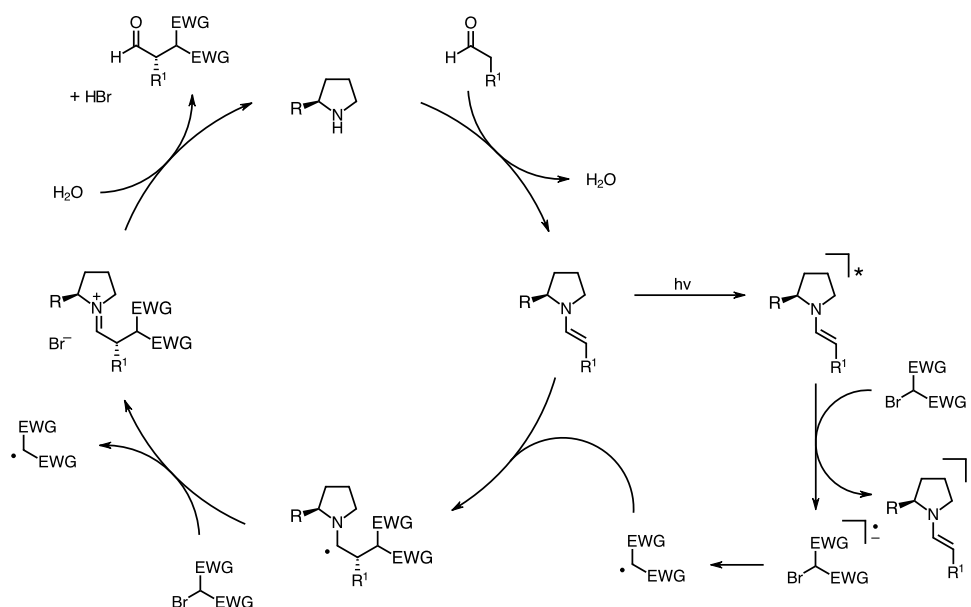


Figure 13: Mechanism of enamine/photocatalysis *via* direct excitation.⁴³

4 Aim of the thesis

The intermolecular direct asymmetric α -alkylation of carbonyl species with alkyl-based electrophiles is owed to its broad synthetic potential among the most important reactions in organic chemistry. Therefore, and as a consequence of many accompanied difficulties, the development of a broadly applicable method remains challenging; thus, in literature, the term “holy grail” is often used.⁴⁴

Nevertheless, as shown in the respective section, many advances have been made within the past few years. Open-shelled methods, especially photocatalytic methods, offer promising potential to achieve this aspiration. While aldehydes have been successfully used as a pronucleophile for versatile intermolecular direct photo and enamine catalytic asymmetric α -alkylation reactions utilizing simple alkyl halides, there are only a few examples for the much less reactive and more challenging ketones.⁷

Motivated by recent advances by Melchiorre *et al.*⁴³ regarding the intermolecular direct asymmetric α -alkylation of aldehydes *via* direct enamine excitation, this thesis aims to investigate a yet unreported sufficient method to translate the discovered reactivity to ketone-based starting materials.

5 Results and discussion

5.1 Reaction design

The recent success of asymmetric enamine catalysis of aldehydes is owed to chiral secondary amino catalysts, primarily based on amino acids, e.g., proline, as they readily form the transient enamine. However, it has been shown that the enamine formation of sterically hindered aldehydes and especially ketones with secondary amines is hindered. This can be rationalized since steric demanding substituents on the N-atom and on the C=C double bond make it more complicated to reach a planar configuration within a tertiary enamine, which is necessary to enable the overlap of the lone pair of the N-atom and the π -system of the C=C double bond. On the other hand, secondary enamines lack one steric demanding substituent, as they bear a comparatively small H-atom instead. Thus, the condensation of primary amines with even sterically hindered carbonyl species is facilitated. As described in the respective section, the secondary enamine is less favored in the equilibrium than the imine. Nevertheless, especially substrates that are inaccessible for secondary amines can be activated with primary amines as secondary enamines.¹⁶

With regard to these considerations and inspired by previous findings particularly by Melchiorre *et al.*⁴¹, the well-established 9-amino(9-deoxy)-*epi*-cinchona alkaloids were assumed to be suitable primary amino catalysts for the aspired transformation. The epimeric substitution (S_N2) of the 9-hydroxy group by an amino group of the highly naturally abundant cinchona alkaloids (quinine, quinidine, cinchonidine, cinchonine) *via* a Mitsunobu-Staudinger reaction yields 9-*epi*-amino cinchona alkaloids that provide a privileged molecular scaffold for asymmetric amino catalysis (Figure 14). As all four representatives feature the same configuration inside the quinuclidine bicycle (*S,S*) and the vinyl substituent (*R*), they are diastereomers. However, as the pair of quinine-NH₂ (**Qn**) and quinidine-NH₂ (**Qd**), respectively cinchonidine-NH₂ (**Cd**) and cinchonine-NH₂ (**Cn**) feature the opposite configuration in the marked positions, they can be considered as “pseudo-enantiomers”. The flexible cinchona alkaloid-based structure allows for high geometrical and facial control within the secondary enamine

formation, thus enforcing high levels of stereocontrol and providing access to both enantiomeric antipodes using both pseudo-enantiomers.^{16, 45}

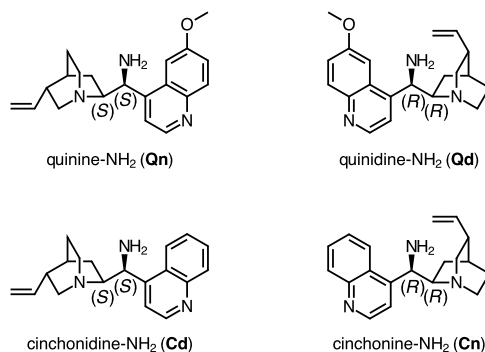
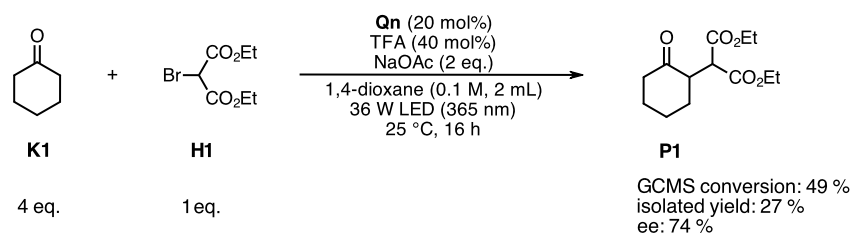


Figure 14: 9-amino(9-deoxy)-*epi*-cinchona alkaloids.¹⁶

The spatial architecture and multifunctional behavior of 9-*epi*-amino cinchona alkaloids, especially the basic quinuclidine moiety and the primary amino functionality, account for their versatile catalytic potential. Under acidic conditions, the most basic tertiary amine is first protonated, which alters the primary amine's electronic properties. As a consequence of electrostatic repulsions, the protonation tendency of the primary amine is reduced, thus guaranteeing a nucleophilic behavior and enhancing the condensation rate with carbonyl species. Furthermore, the protonated quinuclidine moiety can activate electrophiles *via* H-bond interactions, thus providing efficient and spatial approximate reaction conditions for the nucleophilic secondary enamine.¹⁶

Taking these considerations into account, an acidic co-catalyst was found to be necessary to achieve the desired transformation. To avoid regiochemical difficulties accompanied by non-symmetric alkyl substituted ketones, cyclic and symmetric ketones were selected as substrates and cyclohexanone **K1** was chosen as the model substrate. Furthermore, to avoid the formation of diastereomers during the α -alkylation reaction, symmetric and electron-deficient alkyl halides were selected and diethyl bromomalonate **H1** was chosen for the model reaction. Since hydrobromic acid is produced during the α -alkylation reaction, an acid scavenger was necessary to avoid the deactivation of the primary amino catalyst by increased acidic conditions and thus to achieve the desired transformation.

Furthermore, 1,4-dioxane as an aprotic solvent, a universe irradiation wavelength of 365 nm and a typical batch reaction set-up for photochemical reactions were employed. With this reaction design in hand, first attempts were carried out to prove the concept and initial conditions (Scheme 9) were found to synthesize 1,3-diethyl 2-(2-oxocyclohexyl)propanedioate **P1** with good yield and ee.

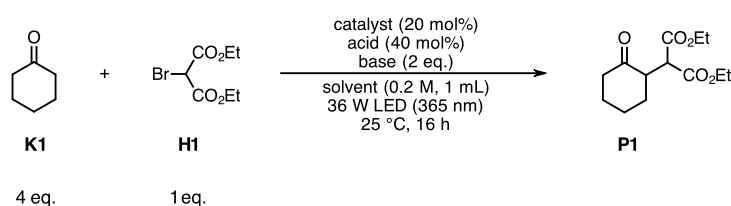


Scheme 9: Initial conditions for synthesizing 1,3-diethyl 2-(2-oxocyclohexyl)propanedioate (**P1**).

5.2 Condition optimization

Encouraged by the successful initial result, the reaction conditions of the model reaction were optimized to improve the yield and ee. Although the GCMS conversion is not equivalent to the isolated yield and does not represent a trustable value, it offers a straightforward method to track trends during condition optimization.

In the GCMS spectra of the crude mixture of diethyl malonate and brominated cyclohexanone, most likely 2-bromocyclohexanone, could be identified beside the desired product and unreacted educts. Standard preparation techniques to establish an inert atmosphere were tested to exclude insufficient inert conditions as a reason for the appearance of these side reactions. However, no significant improvement was observed when argon was passed through the reaction mixture *via* a syringe for a couple of minutes or when degassing the reaction mixture *via* freeze-pump-thaw after the standard preparation using Schlenk technique observed. Interestingly, when carrying out the reaction under the same conditions as stated in Scheme 9 but with doubled concentration (0.2 M, 2 mL), the side reactions could be repressed, thus increasing the GCMS conversion toward the desired product. Optimization of the reaction volume (0.2 M, 1 mL) provided an additional reduction of the side reactions and an additional increase of GCMS conversion towards the desired product. Therefore, this reaction scale was employed for further optimization (Scheme 10).



Scheme 10: Condition optimization of the model reaction.

If the model reaction (Scheme 10) was performed with the other pseudo enantiomer **Qd**, the other enantiomeric antipode of the product was obtained. As a consequence of the diastereomeric nature of the catalysts, they showed different activity. Since **Qd** performed worse (41% GCMS conversion, 18% isolated yield and 72% ee) than **Qn**

under the same conditions as stated in entry 1 of Table 1, **Qn** was primarily taken into the focus for optimization purposes.

5.2.1 Solvent screening

When varying the solvent of the model reaction (Scheme 10) while maintaining NaOAc as an acid scavenger, none of the screening experiments provided an improved GCMS conversion compared to 1,4-dioxane (Table 1, entry 1). On the other hand, toluene gave an improved ee (Table 1, entry 2). A crucial aspect concerning photochemical reactions is the irradiation efficiency. A dispersed solid scatters the light and reduces the light penetration. Since NaOAc was insoluble in all tested solvents, the organic base 2,6-lutidine was chosen to provide homogeneous conditions. Among all tested solvents, DCM (Table 1, entry 9) and DMF (Table 1, entry 10) gave quantitative GCMS conversions and DCM provided an increased ee compared to the initial conditions.

Moreover, in case of DCM and DMF provided homogeneous conditions throughout the entire reaction. When using 2,6-lutidine in combination with the other tested solvents (Table 1, entries 6 to 8), the initially homogeneous solution turned cloudy over time as a consequence of the insolubility of the formed bromide salt. However, when performing the model reaction (Scheme 10) in toluene, an improved ee but a relatively low GCMS conversion was obtained (Table 1, entry 7).

The beneficial behavior of toluene concerning the ee may arise from interactions with the flexible **Qn** moiety and entailed structural modifications.¹⁶ With the aim to exploit the beneficial properties of toluene and DCM in combination with 2,6-lutidine, solvent mixtures were tested. As expected, with an increasing percentage of toluene in DCM, the GCMS conversion decreased and the ee increased. Starting from a 1:1 ratio, the mixture turned heterogeneous after the reaction time. Since the 1:1 mixture only provided a poor cost-to-benefit ratio (64% GCMS conversion and 80% ee), pure DCM in combination with 2,6-lutidine was chosen for further optimization.

Table 1: Solvent screening and comparing the bases NaOAc and 2,6-lutidine in different solvents of the model reaction (Scheme 10).

Entry	Base	Solvent	GCMS conversion (%)	ee (%) ^[a]
1		1,4-Dioxane	88	74
2		Toluene	60	86
3	NaOAc	MTBE	21	82
4		DCM	74	74
5		MeOH	< 5	n.d.
6		1,4-Dioxane	85	76
7		Toluene	48	86
8	2,6-Lutidine	MTBE	53	80
9		DCM	> 95	78
10		DMF	> 95	20

All reactions were performed using **Qn** (20 mol%), **K1** (4 eq.), **H1** (1 eq.), TFA (40 mol%), base (2 eq.), and solvent (0.2 M, 1 mL), 36 W LED (365 nm), 25 °C, 16 h. ^[a]ee was determined on an AS-H column.

5.2.2 Acid and base screening

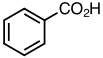
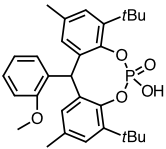
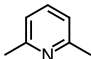
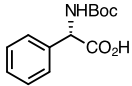
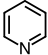
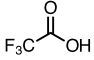
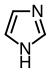
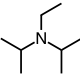
The dual catalytic functionality of 9-*epi*-amino cinchona alkaloids through combined enamine and ion-pairing catalysis allows fine-tuning using a Brønsted acid co-catalyst. The spatial arrangement and the space requirement of an achiral or chiral counter-anion influence the enantioselectivity and catalytic activity *via* tight electrostatic interactions with the protonated quinuclidine moiety.^{16, 46}

With these considerations in mind, different acids were screened. However, when performing the model reaction (Scheme 10) with a weaker acid than TFA (Table 2, entry 1), a sterically demanding and flexible phosphoric acid (Table 2, entry 2) or a chiral phenylalanine-derived acid (Table 2, entry 3) no improvement was observed; thus, TFA was maintained for further studies.

To investigate the effects of different organic bases that provide homogeneous conditions throughout the entire reaction, less sterically hindered aromatic amines than 2,6-lutidine (Table 2, entries 4 and 5) and an aliphatic amine (Table 2, entry 6) were tested. While these bases yielded minor results than 2,6-lutidine, DIPEA showed no reactivity.

A possible explanation for this observation could be the generation of *N*-centered radical cations *via* single electron oxidation of the tertiary amine, the subsequent generation of α -amino alkyl radicals upon deprotonation and several side reactions arranged by these reactive species.⁴⁷

Table 2: Acid and base screening of the model reaction (Scheme 10).

Entry	Acid	Base	GCMS conversion (%)	ee (%) ^[a]
1			44	80
2			92	74
3			88	64
4			60	66
5			73	56
6			n.r.	n.d.

All reactions were performed using **Qn** (20 mol%), **K1** (4 eq.), **H1** (1 eq.), acid (40 mol%), base (2 eq.), DCM (0.2 M, 1 mL), 36 W LED (365 nm), 25 °C, 16 h. ^[a]ee was determined on an AS-H column.

5.2.3 Concentration screening

Interestingly, when performing the model reaction (Scheme 10) without any acid (Table 3, entry 1), no significant decrease in reactivity was observed. Nevertheless, an improved GCMS conversion and ee were obtained if acid was present. This behavior is in accordance with an increased reaction rate and a structural modification of the

9-*epi*-amino cinchona alkaloid in the course of the protonation of the quinuclidine moiety. On the other hand, when performing the reaction without any base (Table 3, entry 3), a dramatically decreased GCMS conversion was observed. If the concentration of cyclohexanone (Table 3, entry 5) or **Qn** (Table 3, entry 6) was reduced to halve its value, the GCMS conversion and thus, the reaction rate was also reduced.

Table 3: Concentration screening of the model reaction (Scheme 10).

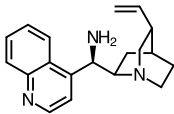
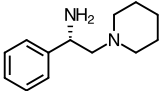
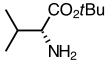
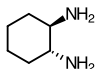
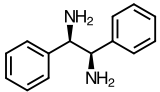
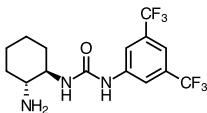
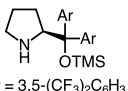
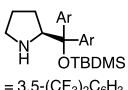
Entry	Variation	GCMS conversion (%)	ee (%) ^[a]
1	TFA (0 mol%)	89	74
2	TFA (20 mol%)	94	76
3	2,6-Lutidine (0 eq.)	18	n.d.
4	2,6-Lutidine (4 eq.)	> 95	78
5	K1 (2 eq.)	83	78
6	Qn (10 mol%)	81	78

All reactions were performed using **Qn** (20 mol%), **K1** (4 eq.), **H1** (1 eq.), TFA (40 mol%), 2,6-lutidine (2 eq.), DCM (0.2 M, 1 mL), 36 W LED (365 nm), 25 °C, 16 h. ^[a]ee was determined on an AS-H column.

5.2.4 Catalyst screening

The model reaction (Scheme 10) was further performed with different catalysts. When using **Cn** (Table 4, entry 1), the identical ee but lower GCMS conversion was obtained compared to **Qn**, indicating that the presence of a methoxy group on the quinoline moiety has a beneficial impact on the activity. The chiral primary amines **PA1** and **PA2** (Table 4, entries 2 and 3), in difference to the chiral vicinal diamines **DA1** and **DA2** (Table 4, entries 4 and 5), yielded the desired product, but with decreased GCMS conversion and ee. No product was obtained with the dual enamine/H-bond catalyst **DC1** (Table 4, entry 6). In accordance with the initial considerations, secondary amino catalysts **SA1** and **SA2** (Table 4, entries 7 and 8) were unable to form the transient enamine. Thus, no GCMS conversion was observed. Notably, the screening reactions stated in entries 7 and 8 of Table 4 were also performed without TFA and under irradiation using a CFL bulb, but no change was observed.

Table 4: Catalyst screening of the model reaction (Scheme 10).

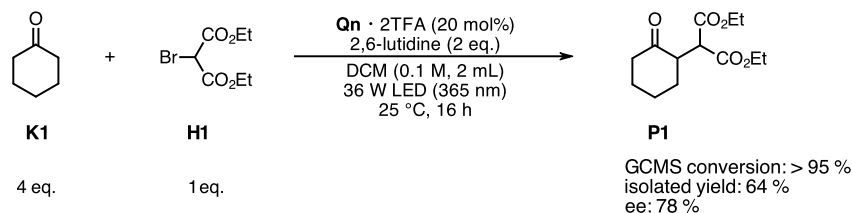
Entry	Catalyst	GCMS conversion (%)	ee (%) ^[a]
1	 Cn	71	78
2	 PA1	62	64
3	 PA2	69	14
4	 DA1	< 5	n.d.
5	 DA2	< 5	n.d.
6	 DC1	< 5	n.d.
7	 SA1 Ar = 3,5-(CF ₃) ₂ C ₆ H ₃	< 5	n.d.
8	 SA2 Ar = 3,5-(CF ₃) ₂ C ₆ H ₃	< 5	n.d.

All reactions were performed using catalyst (20 mol%), **K1** (4 eq.), **H1** (1 eq.), TFA (40 mol%), 2,6-lutidine (2 eq.), DCM (0.2 M, 1 mL), 36 W LED (365 nm), 25 °C, 16 h. ^[a]ee was determined on an AS-H column.

5.2.5 Optimized reaction conditions

The parameter screening resulted in the optimized conditions (Scheme 11), providing quantitative GCMS conversion, 64% isolated yield and 78% ee while guaranteeing homogeneous conditions throughout the entire reaction. The other pseudo enantiomer

Qd again showed decreased activity (38% GCMS conversion, 27% isolated yield and 72% ee) under the same optimized conditions.



Scheme 11: Optimized conditions for synthesizing 1,3-diethyl 2-(2-oxocyclohexyl)propanedioate (**P1**), providing homogeneous conditions throughout the entire reaction.

Since none of the performed screenings managed to combine both a high GCMS conversion, like when the model reaction was performed in DCM and a high ee, like when the model reaction was performed in toluene, a new strategy was followed. With the aim to increase the solubility of **Qn** and to enlarge the steric hindrance, a Ph-group was installed in the 2'-position.

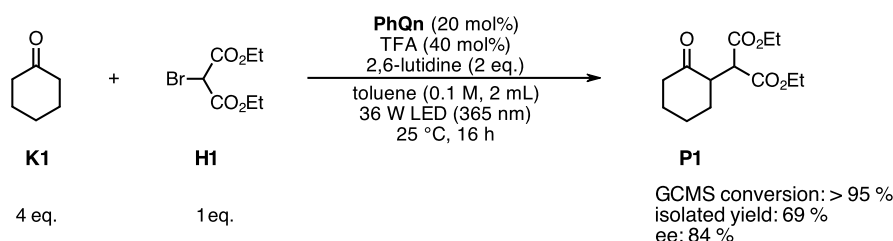
With this derived 9-*epi*-amino cinchona alkaloid – 2'-Ph-quinine-NH₂ (**PhQn**) – in hand, its performance was tested in different solvents. When performing the reaction in DCM (Table 5, entry 1), no improvement compared to **Qn** was observed. However, **PhQn** outperforms **Qn** when using toluene (Table 5, entry 2) since a quantitative GCMS conversion and an improved ee could be obtained. All other tested solvents performed worse regarding the observed GCMS conversion and ee. Nevertheless, DCM was the only tested solvent that guaranteed homogeneous conditions throughout the entire reaction since the reaction mixture became cloudy over time in all other cases.

Table 5: Solvent screening of the model reaction (Scheme 10) performed with **PhQn**.

Entry	Solvent	GCMS conversion (%)	ee (%) ^[a]
1	DCM	> 95	78
2	Toluene	> 95	84
3	1,4-Dioxane	81	74
4	Dibutyl ether	26	65
5	2-Methyltetrahydrofuran	64	70
6	MTBE	87	76

All reactions were performed using **PhQn** (20 mol%), **K1** (4 eq.), **H1** (1 eq.), TFA (40 mol%), 2,6-lutidine (2 eq.), and solvent (0.2 M, 1 mL), 36 W LED (365 nm), 25 °C, 16 h. ^[a]ee was determined on an IA-3 column.

The improved GCMS conversion, isolated yield and ee provided by **PhQn** in combination with toluene as the solvent (Scheme 12) led to improved reaction conditions compared to the previous ones depicted in Scheme 11, but at the expense of homogeneous conditions throughout the entire reaction.



Scheme 12: Optimized conditions for synthesizing 1,3-diethyl 2-(2-oxocyclohexyl)propanedioate (**P1**) at the expense of homogeneous conditions throughout the entire reaction.

Notably, it has been recognized that the ee measured from the crude and isolated products decreased over time. The rationale behind this behavior might be the epimerization as a consequence of the extant acidic α -H atom. The labile stereocenter indicated that the acidic conditions during the work-up and isolation that both relied on flash chromatography using silica may have led to a loss of ee. To verify, the work-up was performed with celite (76% ee) and neutral alumina (55% ee), both yielding as decreased ee compared to the standard method using silica. Also, the saturation of

the acidic silanol groups of the silica with NEt_3 resulted in a dramatic loss of selectivity (38% ee). To decrease the acidity of the α -H atom and prevent epimerization, **P1** was optionally derivatized after the reaction. However, transforming the carbonyl functionality into a hydrazone could not prevent epimerization (80% ee) and a loss of ee over time.

5.3 Mechanistic investigations

5.3.1 Control experiments

Several control experiments were performed under the optimized reaction conditions of the model reaction (Scheme 11). No reactivity was observed when performing the reaction in the presence of TEMPO (Table 6, entry 1), which is a highly efficient free alkyl radical scavenger.⁴⁸ As a consequence of its triplet ground-state, molecular oxygen ($^3\text{O}_2$) can quench the excited photocatalyst's long-lived triplet states (T_1). Furthermore, it can act as a free alkyl radical scavenger, forming peroxy radicals that undergo several side reactions, like hydrogen abstraction or bimolecular termination.⁴⁹ When performing the reaction without providing an inert argon atmosphere (Table 6, entry 2), a dramatically decreased GCMS conversion was observed. These two control experiments verify the presence of a radical reaction mechanism; thus, the strict exclusion of oxygen is crucial. On the other hand, the presence of water (Table 6, entry 3) led to decreased reactivity but no inhibition. When performing the reaction without any irradiation (Table 6, entry 4) or with broader and less focused irradiation spectra, compared to the 36 W LED (365 nm) stripes, using a CFL bulb (Table 6, entry 5), no reactivity was observed. Therefore, the high intensity at 365 nm seems crucial for a successful reaction.

Table 6: Control experiments of the model reaction (Scheme 11).

Entry	Condition	GCMS conversion (%)	ee (%) ^[a]
1	TEMPO (2 eq.)	n.r.	n.d.
2	Air-atmosphere	16	n.d.
3	Water (20 eq.) ^[b]	34	68
4	Dark	n.r.	n.d.
5	CFL bulb	n.r.	n.d.

All reactions were performed using **Qn** (20 mol%), **K1** (4 eq.), **H1** (1 eq.), TFA (40 mol%), 2,6-lutidine (2 eq.), DCM (0.2 M, 1 mL), 36 W LED (365 nm), 25 °C, 16 h. ^[a]ee was determined on an AS-H column. ^[b]1,4-dioxane was used as the solvent.

In order to determine the influence of thermal activation, the model reaction (Scheme 11) was performed without any irradiation. Therefore, the reaction was refluxed in DCM (b.p. = 40 °C). To consider a potentially higher activation barrier, the reaction was refluxed in the higher boiling solvent 1,4-dioxane (b.p. = 101 °C). However, no reactivity was observed in both thermal experiments, thus verifying the necessity of photochemical activation.

5.3.2 UV/Vis spectra

To get further mechanistic insights into the reaction mechanism, UV/Vis spectra of the primary amino catalyst salt in (a) pure form, (b) with the ketone and (c) with the ketone and alkyl halide were measured in DCM as the solvent (Figure 15).

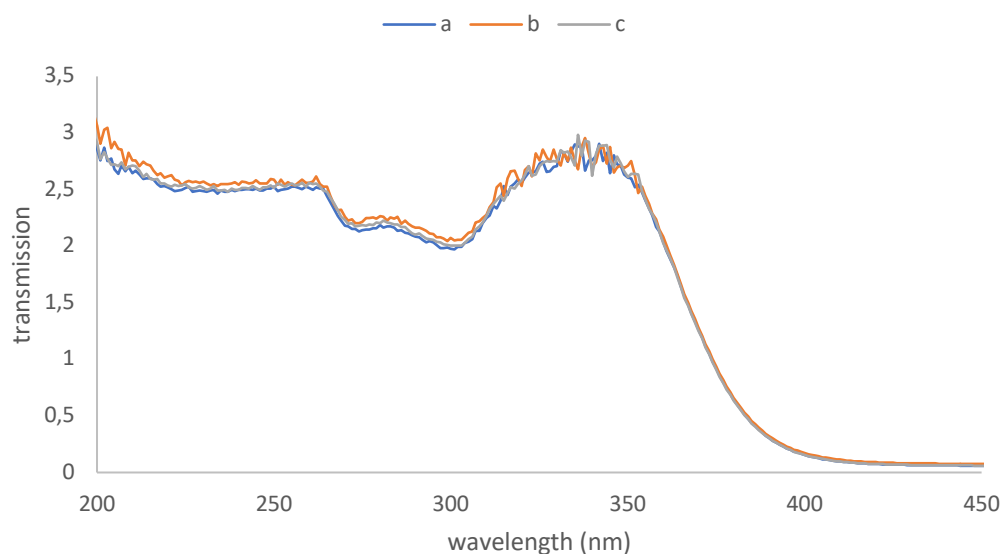


Figure 15: UV/Vis spectra of **Qn** · 2TFA (1 mM) (blue, a), **Qn** · 2TFA (1 mM) plus **K1** (1 mM) (orange, b) and **Qn** · 2TFA (1 mM) plus **K1** (1 mM) plus **H1** (1 mM) (grey, c) in DCM.

Since **Qn** · 2TFA (blue line, a) shows a broad absorption maximum at about 340 nm, the need for such a small irradiation wavelength is revealed. Interestingly, even under acidic conditions, the spectra measured of **Qn** · 2TFA together with cyclohexanone **K1** (orange line, b) looks identical to the pure primary amino catalyst spectra. A possible

explanation for this behavior might be that the condensation reaction is very unfavored and the free amine dominates over any condensation species. Furthermore, the spectra of the mixture of **Qn** · 2TFA, cyclohexanone **K1** and diethyl bromomalonate **H1** (grey line, c) also looks identical to the previously mentioned spectra. Therefore, no shifted absorption behavior is observed and the generation of an EDA complex can be ruled out.

5.3.3 Light on/off experiment

Generally, the product formation in radical reactions can occur *via* a radical-radical coupling or *via* a self-propagating radical chain mechanism. In the latter process, the photocatalyst acts as a photoinitiator and produces initial radicals that form the product within a propagation cycle, regenerating the propagating radical. To distinguish between these two mechanisms, a “light on/off” experiment was performed with the model reaction and under the optimized conditions stated in Scheme 11, whose procedure relies on the alternating on and off switching of the light source (Figure 16).

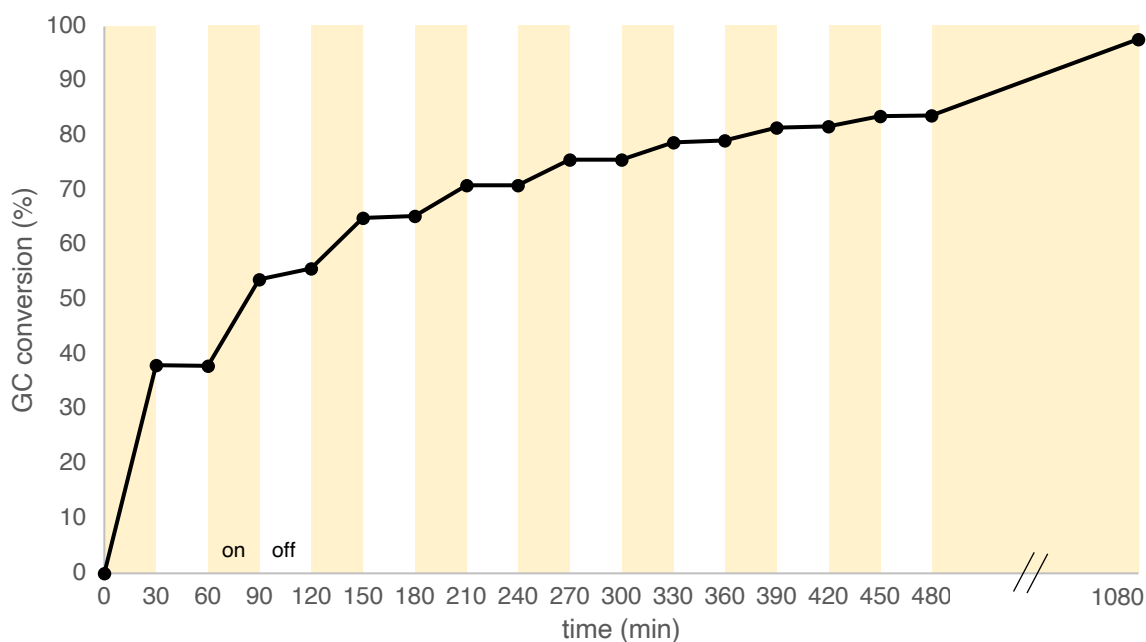


Figure 16: Light on/off experiment.

If the reaction mechanism proceeded *via* a radical chain mechanism, one would expect that during the off periods, the product formation would increase as a consequence of propagating radicals. However, since propagating radicals can be terminated right after the light source is turned off, the constant product formation during the off periods does not rule out a possible radical chain mechanism.⁵⁰

5.3.4 Quantum yield

The more precise method to verify the presence of a radical chain mechanism is the determination of the quantum yield (eq. 1). For an ideal photochemical reaction in which one photon leads to the formation of one product molecule, the quantum yield would be one. In a radical chain mechanism, one photon leads to the formation of more than one molecule; thus, the quantum yield would be larger than one.⁵⁰

$$\Phi(\lambda) = \frac{n_{product}}{n_{photons}} \quad (\text{eq. 1})$$

$\Phi(\lambda)$... quantum yield
λ	... wavelength (nm)
$n_{product}$... amount of substance of product formed (mol)
$n_{photons}$... number of absorbed photons (Einstein)

The ferrioxalate actinometer was selected for the determination of the photon flux of the photoreactor and a quantum yield of 0.63 was measured for the model reaction under the optimized conditions stated in Scheme 11. However, a quantum yield smaller than one does not exclude the presence of a radical chain mechanism as a consequence of non-productive processes, like unimolecular decay processes or an inefficient initiation step.⁵⁰

5.3.5 Proposed mechanism

As a consequence of the observations that the model reaction (i) only proceeds photochemically *via* a radical mechanism, that (ii) no EDA complex formation occurs and that (iii) an enantioenriched product is obtained, direct photoexcitation of the enamine key intermediate and a radical chain mechanism was assumed. The quantum yield smaller than one might be mainly the consequence of the unfavored position of the secondary enamine within the equilibrium and thus, an inefficient initiation step. Since the proposed key intermediate – the enamine – cannot be isolated, no further mechanistic investigations like cyclic voltammetry to determine the redox properties or Stern-Volmer quenching to determine the excited state kinetics could be done.

Notably, a photochemical initiation of the uncondensed 9-amino(9-deoxy)-*epi*-cinchona alkaloid cannot be ruled out. Also, other stereodiscriminating mechanisms based on H-bond or counter-ion catalysis cannot be excluded. However, since other primary amines with different scaffolds than 9-amino(9-deoxy)-*epi*-cinchona alkaloids also lead to the formation of an enantioenriched product in contrast to secondary amines, enamine catalysis is proposed to be dominant. Ultimately, in accordance with the findings of Melchiorre *et al.*⁴³, the following reaction mechanism is proposed (Figure 17).

A part of the transient enamine formed by condensation of cyclohexanone **K1** with **Qn** reaches its excited state upon irradiation and is readily quenched by diethyl bromomalonate **H1**. The alkyl radical is enantioselectively intercepted by the ground-state enamine, subsequent reductive cleavage. The formed α -amino radical triggers the reductive cleavage of diethyl bromomalonate **H1**, regenerating the propagating radical by forming an iminium ion. Upon hydrolysis, **Qn** is regenerated and the α -alkylated product **P1** is released.

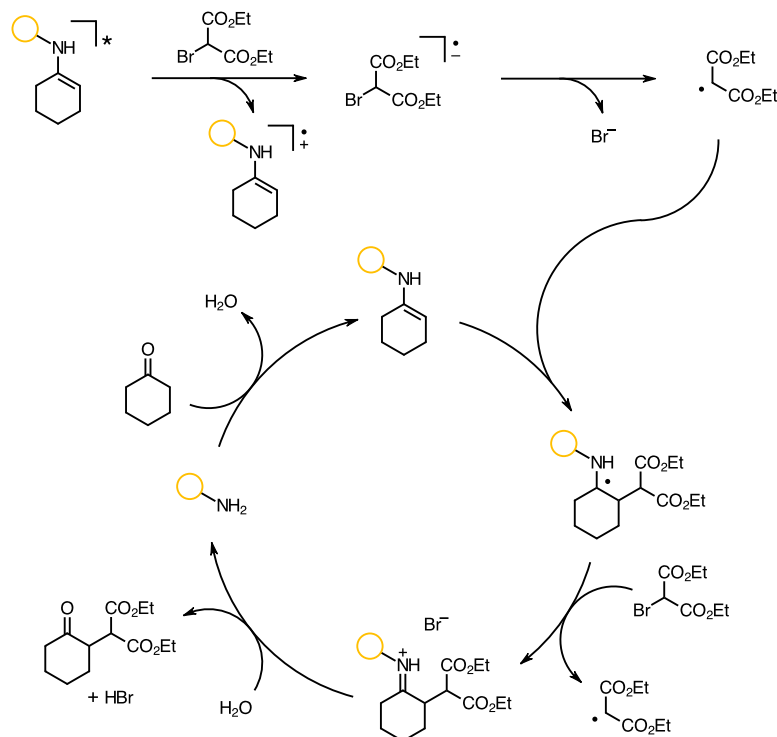


Figure 17: Proposed reaction mechanism of the model reaction (the yellow ring symbolizes the **Qn** moiety).

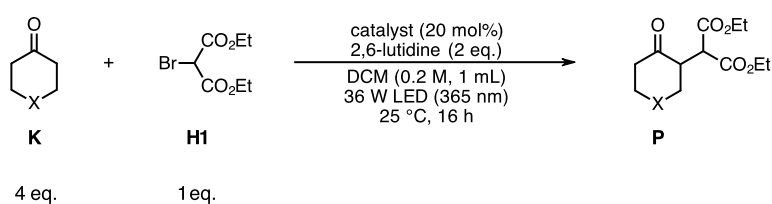
Notably, the initiation step triggered by the excited enamine leads to the formation of an enamine radical cation *via* SET, whose destiny is not connected to any product forming processes; thus, the excited enamine serves as a sacrificial initiator.

5.4 Scope and limitation

With optimized conditions in hand providing homogeneous conditions throughout the entire reaction but at the expense of a reduced ee (Scheme 11) or providing an increased ee but at the expense of the insolubility of the bromide salt (Scheme 12), different ketones and alkyl halides were tested.

5.4.1 Ketones

In accordance with the initial considerations about the avoidance of the generation of regioisomers, different unfunctionalized symmetric cyclic ketones and symmetric 4-functionalized cyclohexanones were evaluated (Scheme 13).

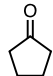
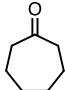
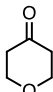
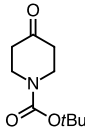
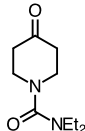
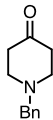
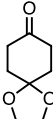


Scheme 13: Optimized reaction conditions for the model reaction applied on different ketones **K**.

All reactions performed under the optimized conditions for the model reaction with **Qn** · 2TFA or **Qd** · 2TFA to provide homogeneous conditions throughout the entire reaction (Scheme 11) were equally homogeneous. Similarly, all reactions performed under the optimized conditions for the model reactions with **PhQn** and toluene as the solvent (Scheme 12) were equally heterogeneous. Despite for all reactions performed with **Qd** · 2TFA a lower GCMS conversion was obtained than with **Qn** · 2TFA, it is not true that always a lower ee was obtained. Nevertheless, the unfunctionalized symmetric and cyclic ketones **K2** (Table 7, entry 1) and **K3** (Table 7, entry 2) seem to follow the same trends as the model substrate **K1** but with worse results. On the other hand, there is no clear trend recognizable for all tested 4-functionalized cyclohexanones, e.g., **K4** with **Qn** · 2TFA (Table 7, entry 3) or **K5** with **Qd** · 2TFA (Table 7, entry 4) provided only a very low ee in sharp contrast to the result obtained with **PhQn**.

Interestingly, the reactions with **PhQn**, **K2** and **K3** (Table 7, entries 1 and 2) provided an increased GCMS conversion and isolated yield but a decreased ee than with **Qn** · 2TFA. On the other hand, for all 4-functionalized cyclohexanones, both an increased reactivity and an increased ee were obtained. Among all tested ketones **K6** (Table 7, entry 5) provided the best ee with **PhQn** and **Qd** · 2TFA to access both enantiomeric antipodes. Notably, the aliphatic amine **K7** (Table 7, entry 4) showed no reactivity, which might have the same reason like for the base DIPEA as discussed above.

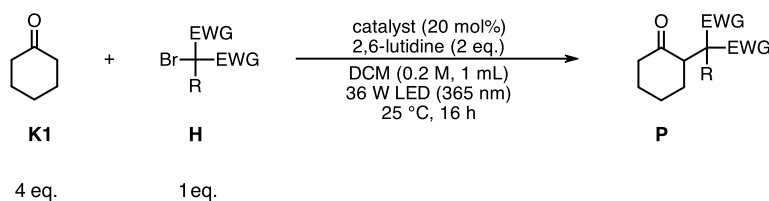
Table 7: Ketone scope (Scheme 13).

Entry	Substrate	Catalyst	GCMS conversion (%)	Yield (%)	ee (%) ^[a]
1	 K2	Qn · 2TFA	71	36	54
		Qd · 2TFA	11	n.d.	38
		PhQn ^[b]	n.d.	49	36
2	 K3	Qn · 2TFA	42	12	40
		Qd · 2TFA	21	n.d.	46
		PhQn ^[b]	n.d.	48	30
3	 K4	Qn · 2TFA	83	51	8
		Qd · 2TFA	57	n.d.	36
		PhQn ^[b]	n.d.	71	82
4	 K5	Qn · 2TFA	94	24 ^[c]	18
		Qd · 2TFA	78	n.d.	4
		PhQn ^[b]	n.d.	16 ^[c]	70
5	 K6	Qn · 2TFA	91	36 ^[c]	64
		Qd · 2TFA	70	n.d.	96
		PhQn ^[b]	n.d.	35 ^[c]	92
6	 K7	Qn · 2TFA	n.r.	n.d.	n.d.
		Qd · 2TFA	n.r.	n.d.	n.d.
		PhQn ^[b]	n.r.	n.d.	n.d.
7	 K8	Qn · 2TFA	77	54	66
		Qd · 2TFA	53	n.d.	76
		PhQn ^[b]	n.d.	86	86

All reactions were performed using catalyst (Qn · 2TFA, Qd · 2TFA or PhQn) (20 mol%), K (4 eq.), H1 (1 eq.), 2,6-lutidine (2 eq.), DCM (0.2 M, 1 mL), 36 W LED (365 nm), 25 °C, 16 h. ^[a]ee was determined on an IA-3 column. ^[b]TFA (40 mol%) was added and toluene (0.2 M, 1 mL) was used as the solvent. ^[c]GCFID yield.

5.4.2 Alkyl halides

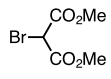
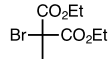
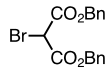
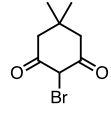
In order to avoid the generation of diastereomers, different symmetric electron-deficient alkyl halides were evaluated (Scheme 14).



Scheme 14: Optimized reaction conditions for the model reaction applied on different alkyl halides **H**.

An increased steric demand of the alkyl halide compared to the model substrate **H1** or **H2** (Table 8, entry 1) resulted in a low reactivity (Table 8, entries 2 and 3) or no reactivity at all (Table 8, entry 4). All reactions performed under the optimized conditions for the model reaction with **Qn** · 2TFA or **Qd** · 2TFA to provide homogeneous conditions throughout the entire reaction (Scheme 11) were equally homogeneous. Similarly, all reactions performed under the optimized conditions for the model reactions with **PhQn** and toluene as the solvent (Scheme 12) were equally heterogeneous. Although the reaction of **H2** (Table 8, entry 1) performed with **Qn** · 2TFA and **PhQn** showed equally to the model substrate **H1** quantitative GCMS conversion, a lower isolated yield and ee were obtained. However, the general trend was in accordance with the model reaction.

Table 8: Alkyl halide scope (Scheme 14).

Entry	Substrate	Catalyst	GCMS conversion (%)	Yield (%)	ee (%) ^[a]
1	 H2	Qn · 2TFA	> 95	50	51
		Qd · 2TFA	84	n.d.	45
		PhQn ^[b]	> 95	61	80
2	 H3	Qn · 2TFA	< 5	n.d.	n.d.
		Qd · 2TFA	< 5	n.d.	n.d.
		PhQn ^[b]	< 5	n.d.	n.d.
3	 H4	Qn · 2TFA	< 5	n.d.	n.d.
		Qd · 2TFA	< 5	n.d.	n.d.
		PhQn ^[b]	n.d.	n.d.	n.d.
4	 H5	Qn · 2TFA	n.r.	n.d.	n.d.
		Qd · 2TFA	n.r.	n.d.	n.d.
		PhQn ^[b]	n.d.	n.d.	n.d.

All reactions were performed using catalyst (**Qn** · 2TFA, **Qd** · 2TFA or **PhQn**) (20 mol%), **K1** (4 eq.), **H** (1 eq.), 2,6-lutidine (2 eq.), DCM (0.2 M, 1 mL), 36 W LED (365 nm), 25 °C, 16 h. ^[a]ee was determined on an IA-3 column. ^[b]TFA (40 mol%) was added and toluene (0.2 M, 1 mL) was used as the solvent.

5.5 Continuous-flow implementation

5.5.1 Overview

Over the past decades, continuous-flow based synthesis techniques underwent flourishing investigation. As a consequence of many advantages, such as improved mixing, more efficient temperature control, facile scalability or increased safety, they have been applied for various synthetic applications.⁵¹

The implementation of photochemical reactions into continuous-flow systems not only increases its overall efficiency but also overcomes inherent limitations. According to the Lambert-Beer law, the light penetration through the reaction solution diminishes with increasing depth by absorption; thus, batch reactions that typically suffer from a deficient mass transport cannot be scaled up efficiently as a consequence of non-uniform irradiation. This problem is overcome by thin and light-permeable tubes coiled around the light source of continuous-flow systems, providing short path lengths for a facile and uniform light penetration of the reaction solution. In contrast to batch reactors, continuous-flow systems are not scaled up by enlarging the reaction volume but by prolonging the reaction time. Also, as a consequence of the miniaturization, mass and heat transfer in continuous-flow systems are accomplished more efficiently than in batch reactors, and facile temperature control and improved selectivity is enabled. These benefits, together with the high spatiotemporal control to guarantee sufficient irradiation, make continuous-flow predetermined for photochemical reactions.^{52, 53}

5.5.2 Screening of conditions

Implementing the model reaction into continuous-flow required homogeneous conditions throughout the entire reaction to avoid tubing blockage. Therefore, **Qn** · 2TFA in combination with DCM as the solvent was chosen for the continuous-flow optimization of the model reaction (Scheme 11). All continuous-flow experiments were performed using a Vapourtec E-Series with a UV-150 photochemical reactor. As depicted in the flow diagram (Figure 18), the reaction solution was stored in a vial under argon, pumped through the photoreactor (10 mL volume) and collected in a second vessel. The back pressure was controlled by a second pump set as a back pressure regulator.

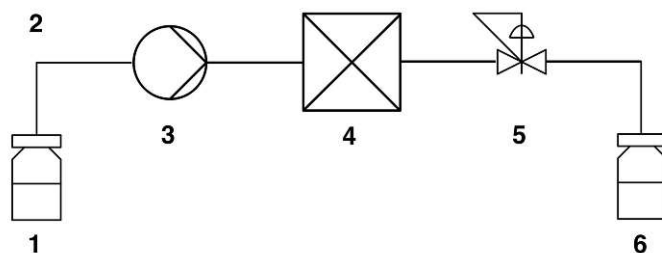
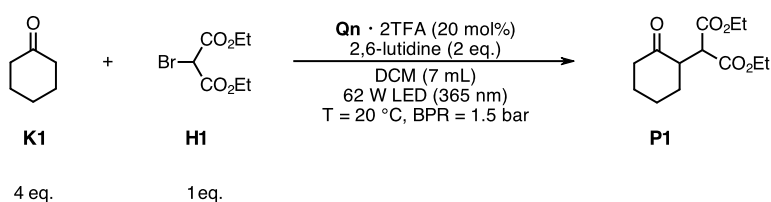


Figure 18: Flow diagram of the flow photoreactor (1: reaction solution, 2: tubing, 3: pump, 4: photoreactor, 5: back pressure regulator, 6: collector).

All continuous-flow experiments were performed using the optimized conditions providing homogeneous conditions throughout the entire reaction (Scheme 11), setting the back pressure to 1.5 bar, the temperature to 20 °C and using a volume of 7 mL of the reaction mixture (Scheme 15).



Scheme 15: Reaction conditions of the model reaction applied for continuous-flow experiments.

During the continuous-flow optimization, the LED power (%), the reaction solution concentration (M, regarding the limiting component) and the flow rate ($\mu\text{L}/\text{min}$) were varied. A lower LED Power of 50% and a higher flow rate of 500 $\mu\text{L}/\text{min}$ and thus a shorter residence time influenced the reaction positively (Table 9, entries 4 and 5). The rationale behind this behavior might be an over-irradiation of the reaction solution by the more powerful LED compared to the LED stripes used in the batch photoreactor. Interestingly, a low concentration of 0.05 M (Table 9, entries 1 and 2) and a high concentration of 0.20 M (Table 9, entries 5 and 6) lead to a lower GCMS conversion and ee than a medium concentration of 0.10 M (Table 9, entries 3 and 4). It is worth mentioning that the retention time of all experiments, which could be easily tracked as a consequence of the colored reaction solution, differed from the theoretical retention time, which was calculated from the flow rate and the reactor volume. Probably the

main reason for this behavior was the generation of bubbles within the reaction solution coming out of the photoreactor that interfered with the pump system. However, the most promising result was achieved with the conditions stated in entry 4 of Table 9, producing the desired product with high productivity and good ee. In this regard, testing other solvents with high boiling points and low dielectric constants (e.g., 1,4-dioxane) is envisioned to address the most likely viscosity-related bubble generation.

Table 9: Continuous-flow optimization of the model reaction (Scheme 15).

Entry	LED power (%)	c (M)	flow rate ($\mu\text{L}/\text{min}$)	GCMS conversion (%)	Productivity (mmol/h)	ee (%) ^[a]
1	100	0.05	500	31	0.47	74
2	100	0.05	333	24	0.24	72
3	100	0.10	500	46	1.38	76
4	50	0.10	500	57	1.71	78
5	50	0.20	500	55	3.30	54
6	50	0.20	333	46	1.84	54

All reactions were performed using **Qn** · 2TFA (20 mol%), **K1** (4 eq.), **H1** (1 eq.), 2,6-lutidine (2 eq.), DCM (c, 7 mL), 62 W LED (365 nm), 20 °C, 1.5 bar BPR. ^[a]ee was determined on an AS-H column.

6 Conclusion and outlook

This thesis reported a new method for the direct intermolecular photo/organocatalytic asymmetric α -alkylation of symmetric and cyclic ketones with symmetric electron-deficient alkyl halides.

Initial considerations about the necessity of primary amino catalysts to transiently form a secondary enamine with sterically demanding ketones were verified. Among all tested primary amino catalysts, 9-amino(9-deoxy)-*epi*-cinchona alkaloids were the most active for the model reaction. The necessity of the 365 nm irradiation was explained by UV/Vis measurements, unveiling that no EDA complex formation occurs. The determined quantum yield lower than one might result from the unfavored secondary enamine formation. Thus, a self-propagating radical chain reaction initiated by the direct secondary enamine photoexcitation is proposed as a reaction mechanism.

The acidic co-catalyst TFA was discovered to be beneficial for the reaction rate, but no increased activity as a consequence of spatial effects of the counter-ion was found to be involved. An acid scavenger for the hydrobromic acid formed during the reaction was found to be crucial, which might originate from the deactivation of the primary amino catalyst. 2,6-Lutidine showed the best results as a consequence of its solubility in organic solvents. **Qn** (respectively **PhQn**) was among all tested 9-amino(9-deoxy)-*epi*-cinchona alkaloids the most active primary amino catalyst for the model reaction, whereas the other enantiomeric antipode was accessible with its pseudo enantiomer **Qd**.

It was discovered that the model reaction performed with **Qn** and DCM as the solvent provided quantitative GCMS conversion, a good ee and homogeneous conditions throughout the entire reaction (Scheme 11). With toluene as the solvent, a decreased GCMS conversion and an improved ee but heterogeneous conditions as a consequence of the formed hydrobromic salt were provided. With the establishment of **PhQn**, a quantitative GCMS conversion and an improved ee at the expense of heterogeneous reaction conditions were achieved with toluene as the solvent (Scheme 12).

The discovered optimized reaction conditions were transferred to other diverse functionalized ketones and alkyl halides to synthesize the respective α -alkylated products

with good yield and ee in batch conditions. The optimized reaction conditions providing homogeneous conditions throughout the entire reaction were further applied for the implementation into continuous-flow (Scheme 15), producing the α -alkylated product of the model reaction with good productivity and ee.

Although not included in this thesis anymore, research on this topic is ongoing. Attempts will also be made to transfer the synthesis of the presented and the prospective enlarged scope into continuous-flow and to determine the absolute configuration of all α -alkylated ketones.

7 Experimental Part

7.1 Materials and methods

All chemicals used for synthesis were purchased from commercial suppliers with a purity greater than 95% or were available in the laboratory from colleagues^{54, 55} and were used without further purification. Anhydrous solvents were pre-distilled and desiccated on aluminum oxide using a PureSolv purification system by Innovative Technology or were purchased from commercial suppliers and stored in septum-closed bottles.

For preparative flash chromatography, manual glass columns and Merck silica (40 to 60 μm) were used, and the column size and the eluent were adapted to the respective separation problem. Solvent compositions for elution or reaction purposes are stated as volume ratios. TLC analysis for reaction and elution monitoring was performed using precoated aluminum-backed silica 60 F₂₅₄ plates purchased from Merck. The spot visualization was achieved using UV light (254 nm) for UV active compounds and staining solutions for non-UV active compounds. The following staining agents were used:

Anisaldehyde: Ethanol (135 mL) plus concentrated sulfuric acid (5 mL) plus glacial acetic acid (1.5 mL) plus *p*-anisaldehyde (3.7 mL).

Ninhydrin: *n*-Butanol (100 mL) plus ninhydrin (1.5 g) plus concentrated acetic acid (3 mL).

Vanillin: Ethanol (250 mL) plus vanillin (15 g) plus concentrated sulfuric acid (2.5 mL).

NMR spectra were recorded at 297 K on a Bruker Advance UltraShield (¹H: 400 MHz) spectrometer. Chemical shifts (δ) were reported in ppm with TMS as an internal standard by calibration to the respective solvent signal and coupling constants (*J*) were reported in Hz. Deuterated solvents were purchased from commercial suppliers and stored over molecular sieve. The following abbreviations are used in the NMR codes to explain multiplicities: s (singlet), d (doublet), t (triplet), q (quartet), combinations thereof and m (multiplet).

GC measurements were performed on a Thermo Scientific Focus on a BGB5 column equipped with an FID detector.

GCMS measurements were performed on a Thermo Scientific DSQ II on a BGB5 column equipped with a quadrupole MS detector.

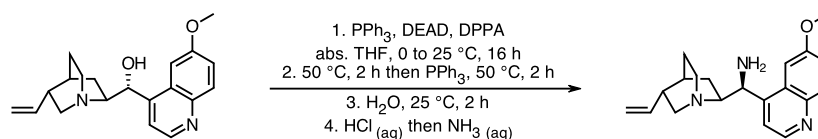
Chiral HPLC measurements were performed on a DIONEX UPLC equipped with a photodiode array detector (190 to 360 nm), and columns from Diacel Chiracel AS-H and IA-3 (all 250 × 4.60 mm, 5 μm) were used.

Infrared spectra were recorded at 297 K on a Perkin-Elmer Spectrum 65 FT-IR spectrometer equipped with a specac MK II Golden Gate Single Reflection ATR unit.

UV/Vis spectra were recorded at 297 K on a Shimadzu UV/Vis 1800 spectrometer using 1 cm path length quartz cuvettes.

7.2 Catalyst synthesis

7.2.1 (8 α ,9S)-6'-Methoxycinchonan-9-amine (Qn)



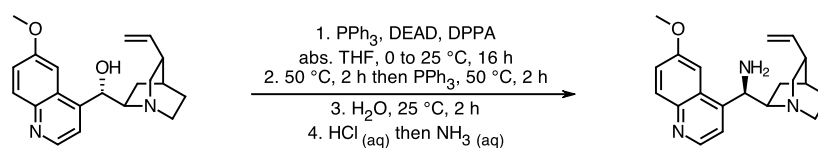
Quinine (3.24 g, 10.0 mmol, 1.0 eq.) and PPh₃ (3.15 g, 12.0 mmol, 1.2 eq.) were placed in a 100 mL three-neck round bottle flask equipped with a dropping funnel and a condenser and dissolved in anhydrous THF (50 mL). The colorless solution was cooled to 0 °C with an ice bath and DEAD (2.09 g, 12.0 mmol, 1.2 eq.) was added *via* syringe while stirring. DPPA (3.30 g, 12.0 mmol, 1.2 eq.) was placed in the dropping funnel, dissolved in anhydrous THF (10 mL) and slowly added at 0 °C. The yellow solution was stirred at room temperature for 16 h and then stirred at 50 °C for 2 h. PPh₃ (3.42 g, 13.0 mmol, 1.3 eq.) was added in portions at 50 °C under the generation of N₂. The yellow solution was stirred at 50 °C for 2 h, distilled H₂O (1 mL) was added at room temperature and the reaction mixture was stirred at room temperature for additional 2 h. The reaction mixture was transferred into a 250 mL one-neck round bottle flask and the solvent was removed under vacuum. Subsequently, 10% HCl_(aq) (100 mL) and DCM (100 mL) were added to the yellow liquid residue and after the phase separation, the aqueous phase was extracted three times with DCM (20 mL). The aqueous phase was evaporated, and traces of water were removed by dissolving the yellow solid residue in MeOH (20 mL), followed by evaporation for three times. The yellow solid residue was dissolved in MeOH (40 mL), the yellow solution was refluxed and EtOAc (100 mL) was added to precipitate the hydrochloric amine salt. The solid was filtrated and washed with EtOAc. The obtained yellow solid was dissolved in DCM (50 mL) and 5 M NH₃_(aq) (15 mL) was added. After the phase separation, the aqueous phase was extracted three times with DCM (20 mL), and the combined organic phases were washed with brine, dried over anhydrous MgSO₄, filtrated and evaporated.

(8 α ,9S)-6'-Methoxycinchonan-9-amine **Qn** was obtained as an orange oily liquid (2.59 g, 8.01 mmol, 80%).

¹H NMR (400 MHz, CDCl₃) δ 8.75 (d, *J* = 4.5 Hz, 1H), 8.03 (d, *J* = 9.2 Hz, 1H), 7.66 (s, 1H), 7.49 – 4.42 (m, 1H), 7.39 (dd, *J* = 9.2, 2.7 Hz, 1H), 5.80 (ddd, *J* = 17.5, 10.3, 7.5 Hz, 1H), 5.06 – 4.93 (m, 2H), 4.65 – 4.54 (m, 1H), 3.97 (s, 3H), 3.28 (dd, *J* = 13.8, 10.0 Hz, 1H), 3.25 – 3.16 (m, 1H), 3.14 – 3.07 (m, 1H), 2.86 – 2.75 (m, 2H), 2.34 – 2.24 (m, 1H), 1.95 (s, 2H), 1.64 – 1.60 (m, 1H), 1.58 – 1.51 (m, 2H), 1.48 – 1.36 (m, 1H), 0.81 – 0.73 (m, 1H).

Analytical data was in accordance with literature.⁴⁵

7.2.2 (9*R*)-6'-Methoxycinchonan-9-amine (Qd)



Quinidine (3.24 g, 10.0 mmol, 1.0 eq.) and PPh₃ (3.15 g, 12.0 mmol, 1.2 eq.) were placed in a 100 mL three-neck round bottle flask equipped with a dropping funnel and a condenser and dissolved in anhydrous THF (50 mL). The colorless solution was cooled to 0 °C with an ice bath and DEAD (2.09 g, 12.0 mmol, 1.2 eq.) was added *via* syringe while stirring. DPPA (3.30 g, 12.0 mmol, 1.2 eq.) was placed in the dropping funnel, dissolved in anhydrous THF (10 mL) and slowly added at 0 °C. The yellow solution was stirred at room temperature for 16 h and then stirred at 50 °C for 2 h. PPh₃ (3.42 g, 13.0 mmol, 1.3 eq.) was added in portions at 50 °C under the generation of N₂. The yellow solution was stirred at 50 °C for 2 h, distilled H₂O (1 mL) was added at room temperature and the reaction mixture was stirred at room temperature for additional 2 h. The reaction mixture was transferred into a 250 mL one-neck round bottle flask and the solvent was removed under vacuum. Subsequently, 10% HCl_(aq) (100 mL) and DCM (100 mL) were added to the yellow liquid residue, and after the phase separation, the aqueous phase was extracted three times with DCM (20 mL). The aqueous phase was evaporated, and traces of water were removed by suspending the yellow solid residue in MeOH (20 mL), followed by evaporation for three times. The yellow solid residue was suspended in MeOH (80 mL), the yellow suspension was refluxed and EtOAc (100 mL) was added to reduce the solubility of the hydrochloric amine salt. The solid was filtrated and washed with EtOAc. The obtained yellow solid was dissolved in DCM (50 mL) and 5 M NH₃_(aq) (15 mL) was added. After the phase separation, the aqueous phase was extracted three times with DCM (20 mL), and the combined organic phases were washed with brine, dried over anhydrous MgSO₄, filtrated and evaporated.

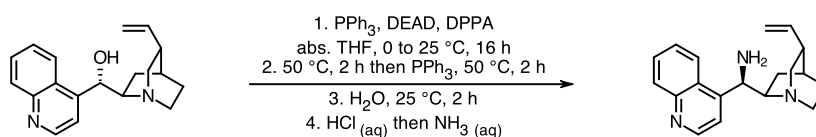
(9*R*)-6'-Methoxycinchonan-9-amine **Qd** was obtained as an orange oily liquid (1.52 g, 4.69 mmol, 47%).

¹H NMR (400 MHz, CDCl₃) δ 8.75 (d, *J* = 4.6 Hz, 1H), 8.02 (d, *J* = 9.2 Hz, 1H), 7.61 (s, 1H), 7.56 – 7.48 (m, 1H), 7.38 (dd, *J* = 9.2, 2.7 Hz, 1H), 5.89

(ddd, $J = 17.1, 10.6, 6.5$ Hz, 1H), 5.12 – 5.02 (m, 2H), 4.73 – 4.59 (m, 1H), 3.97 (s, 3H), 3.11 – 2.87 (m, 5H), 2.33 – 2.24 (m, 1H), 1.94 (s, 2H), 1.64 – 1.58 (m, 1H), 1.58 – 1.48 (m, 2H), 1.18 – 1.10 (m, 1H), 1.01 – 0.91 (m, 1H).

Analytical data was in accordance with literature.⁴⁵

7.2.3 (9*R*)-Cinchonan-9-amine (Cn)



Cinchonine (2.94 g, 10.0 mmol, 1.0 eq.) and PPh₃ (3.93 g, 15.0 mmol, 1.5 eq.) were placed in a 150 mL tree neck round bottle flask equipped with a dropping funnel and a condenser and suspended in anhydrous THF (50 mL). The colorless suspension was cooled to 0 °C with an ice bath and DEAD (2.61 g, 15.0 mmol, 1.5 eq.) was added *via* syringe while stirring. DPPA (4.13 g, 15.0 mmol, 1.5 eq.) was placed in the dropping funnel, dissolved in anhydrous THF (20 mL) and slowly added at 0 °C. The reaction mixture turned homogeneous while stirring at room temperature for 16 h. Afterward, the yellow solution was stirred at 50 °C for 2 h, and PPh₃ (6.58 g, 25.1 mmol, 2.5 eq.) was added at 50 °C in portions under the generation of N₂. The yellow solution was stirred at 50 °C for 2 h, distilled H₂O (3 mL) was added at room temperature and the reaction mixture was stirred at room temperature for additional 16 h. The reaction mixture was transferred into a 250 mL one-neck round bottle flask and the solvent was removed under vacuum. Subsequently, 10% HCl_(aq) (80 mL) and DCM (80 mL) were added to the yellow liquid residue and after the phase separation, the aqueous phase was extracted three times with DCM (20 mL). 5 M NH₃_(aq) was added to the aqueous phase until a pH of 9 was reached. After adding DCM (80 mL) to the basic aqueous phase, the phases were separated, and the aqueous phase was extracted three times with DCM (40 mL). The combined organic phases were washed with brine, dried over anhydrous MgSO₄, filtrated and evaporated. The brown crude product was purified *via* flash chromatography (silica, EtOAc:MeOH:NH₃_(aq) = 50:50:1, ninhydrin staining agent).

(9*R*)-Cinchonan-9-amine **Cn** was obtained as an orange oily liquid (1.68 g, 5.73 mmol, 57%).

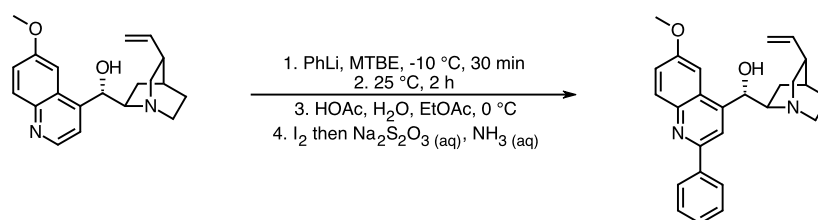
¹H NMR (400 MHz, CDCl₃) δ 8.90 (d, *J* = 4.5 Hz, 1H), 8.42 – 8.29 (m, 1H), 8.14 (dd, *J* = 8.3, 1.3 Hz, 1H), 7.72 (ddd, *J* = 8.4, 6.8, 1.4 Hz, 1H), 7.59 (ddd, *J* = 8.6, 5.4, 1.5 Hz, 2H), 5.86 (ddd, *J* = 16.9, 10.8, 6.8 Hz, 1H), 5.11 – 5.03 (m, 2H), 4.82 – 4.69 (m, 1H), 3.10 – 2.88 (m, 5H), 2.32 – 2.21 (m,

1H), 1.91 (s, 2H), 1.63 – 1.49 (m, 3H), 1.17 – 1.06 (m, 1H), 1.01 – 0.89 (m, 1H).

¹³C NMR (101 MHz, CDCl₃) δ 150.43 (s), 149.15 (s), 148.67 (s), 140.73 (s), 130.55 (s), 129.12 (s), 127.99 (s), 126.50 (s), 123.47 (s), 119.79 (s), 114.64 (s), 62.37 (s), 53.54 (s), 49.67 (s), 47.56 (s), 39.79 (s), 27.80 (s), 26.84 (s), 25.16 (s).

Analytical data was in accordance with literature.⁵⁶

7.2.4 (9S)-6'-Methoxy-2'-phenylcinchonan-9-ol

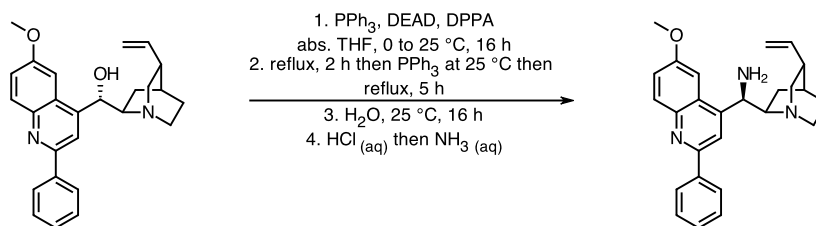


Quinidine (3.00 g, 9.25 mmol, 1.0 eq.) was placed into an oven-dried 250 mL three-neck round bottle flask equipped with an argon-filled balloon and a condenser and was suspended in anhydrous MTBE (60 mL) under an argon atmosphere. The suspension was cooled to -10 °C with an ice/NaCl bath and PhLi (1.90 M in Bu₂O, 14.6 mL, 27.3 mmol, 3.0 eq.) was added *via* syringe through a septum during vigorous stirring. The brownish reaction mixture was stirred at -10 °C for 30 min and at room temperature for 2 h. Afterward, it was cooled to 0 °C with an ice bath and concentrated acetic acid (7.5 mL) was slowly added *via* syringe through a septum. Distilled H₂O (25 mL) and EtOAc (25 mL) were added at 0 °C, and I₂ was added in portions at room temperature to the biphasic system until a dark color remained. The dark biphasic system turned yellow, and a solid precipitated after adding 0.5 M Na₂S₂O₃ (25 mL). While vigorous stirring, concentrated NH₃ (aq) (15 mL) was added, dissolving the solid and the yellow biphasic system was stirred at room temperature for 10 min. After the phase separation, the organic phase was washed with brine, and the combined aqueous phases were extracted three times with DCM (40 mL). The combined organic phases were dried over anhydrous MgSO₄, filtrated and evacuated. The yellow solid crude product was purified *via* flash chromatography (silica, PE:EtOAc:MeOH:NEt₃ = 8:1:0.5:0.5, ninhydrin staining agent).

(9S)-6'-Methoxy-2'-phenylcinchonan-9-ol was obtained as a yellow solid (2.64 g, 6.60 mmol, 71%).

¹H NMR (400 MHz, CDCl₃) δ 8.08 – 8.03 (m, 3H), 7.93 (s, 1H), 7.49 – 7.38 (m, 3H), 7.32 (dd, *J* = 9.2, 2.7 Hz, 1H), 7.13 (d, *J* = 2.8 Hz, 1H), 6.09 – 5.98 (m, 1H), 5.61 (d, *J* = 4.1 Hz, 1H), 5.09 – 5.00 (m, 2H), 3.87 (s, 3H), 3.40 – 3.31 (m, 1H), 3.08 (td, *J* = 9.3, 4.1 Hz, 1H), 2.98 – 2.86 (m, 2H), 2.83 – 2.73 (m, 1H), 2.24 (q, *J* = 8.5 Hz, 1H), 2.10 – 2.02 (m, 1H), 1.79 – 1.72 (m, 1H), 1.57 – 1.44 (m, 3H), 1.23 – 1.13 (m, 1H).

7.2.5 (9*R*)-6'-Methoxy-2'-phenylcinchonan-9-amine (PhQd)



(9*S*)-6'-Methoxy-2'-phenylcinchonan-9-ol (2.35 g, 5.88 mmol, 1.0 eq.) and PPh₃ (1.89 g, 7.05 mmol, 1.2 eq.) were placed in a 250 mL three-neck round bottle flask equipped with a dropping funnel and a condenser and dissolved in anhydrous THF (50 mL). The colorless solution was cooled to 0 °C with an ice bath and DEAD (1.29 g, 7.05 mmol, 1.2 eq.) was added *via* syringe while stirring. DPPA (2.00 g, 7.05 mmol, 1.2 eq.) was placed in the dropping funnel, dissolved in anhydrous THF (10 mL) and slowly added at 0 °C. The yellow solution was stirred at room temperature for 16 h and was refluxed afterward for 2 h. PPh₃ (1.89 g, 7.05 mmol, 1.2 eq.) was added in portions at room temperature under the generation of N₂. The yellow solution was refluxed for 2 h, distilled H₂O (12 mL) was added at room temperature and the reaction mixture was stirred at room temperature for 16 h. The reaction mixture was transferred into a 250 mL one-neck round bottle flask and the solvent was removed under vacuum. 10% HCl (aq) (30 mL) and DCM (30 mL) were added to the yellow liquid residue and after the phase separation, the aqueous phase was extracted three times with DCM (20 mL). 5 M NH₃ (aq) was added to the aqueous phase until a pH of 9 was reached. After adding DCM (50 mL) to the basic aqueous phase, the phases were separated, and the aqueous phase was extracted three times with DCM (30 mL). The combined organic phases were dried over anhydrous MgSO₄, filtrated and evaporated.

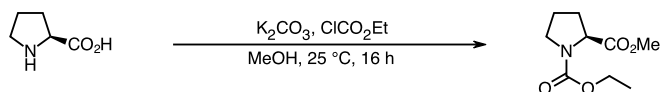
(9*R*)-6'-Methoxy-2'-phenylcinchonan-9-amine **PhQd** was obtained as a yellow solid (1.78 g, 4.44 mmol, 76%).

¹H NMR (400 MHz, CDCl₃) δ 8.20 – 8.13 (m, 2H), 8.10 (d, *J* = 9.2 Hz, 1H), 8.07 (s, 1H), 7.51 (tq, *J* = 6.1, 1.3 Hz, 3H), 7.48 – 7.39 (m, 1H), 7.39 (dd, *J* = 9.2, 2.8 Hz, 1H), 5.91 (ddd, *J* = 17.1, 10.6, 6.5 Hz, 1H), 5.14 – 5.02 (m, 2H), 4.75 (d, *J* = 9.9 Hz, 1H), 3.98 (s, 3H), 3.13 – 2.90 (m, 7H), 2.30 (q,

$J = 7.9$ Hz, 1H), 1.63 (s, 1H), 1.60 – 1.49 (m, 2H), 1.27 – 1.16 (m, 1H),
1.05 – 0.93 (m, 1H).

Analytical data was in accordance with literature.⁵⁷

7.2.6 (2S)-1,2-Pyrrolidinedicarboxylic acid 1-ethyl 2-methyl ester



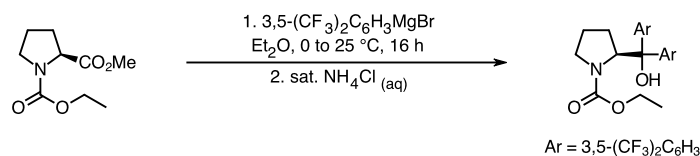
L-Proline (3.03 g, 26.1 mmol, 1.0 eq.) and K₂CO₃ (3.60 g, 26.1 mmol, 1.0 eq.) were placed in a 100 mL three-neck round bottle flask equipped with a condenser and suspended in MeOH (40 mL). Ethyl chloroformate (6.35 g, 57.3 mmol, 2.2 eq.) was added *via* syringe and the suspension was stirred at room temperature for 16 h. The suspension was transferred to a 500 mL one-neck round bottle flask and the solvent was removed under vacuum. The white solid residue was dissolved in distilled H₂O (200 mL) and DCM (100 mL). After the phase separation, the aqueous phase was extracted three times with DCM (100 mL), and the combined organic phases were washed with brine, dried over anhydrous MgSO₄, filtrated and evaporated.

(2S)-1,2-Pyrrolidinedicarboxylic acid 1-ethyl 2-methyl ester was obtained as a colorless liquid (5.21 g, 24.8 mmol, 95%).

¹H NMR (400 MHz, CDCl₃) δ 4.36 (dd, *J* = 8.6, 3.5 Hz, 1H), 4.29 (dd, *J* = 8.6, 3.9 Hz, 1H), 4.20 – 4.01 (m, 4H), 3.73 (s, 3H), 3.71 (s, 3H), 3.64 – 3.39 (m, 4H), 2.30 – 2.11 (m, 2H), 2.07 – 1.81 (m, 6H), 1.26 (t, *J* = 7.1 Hz, 3H), 1.19 (t, *J* = 7.1 Hz, 3H).

Analytical data was in accordance with literature.⁵⁸

7.2.7 (2S)-2-[Bis[3,5-bis(trifluoromethyl)phenyl]hydroxymethyl]-1-pyrrolidinecarboxylic acid ethyl ester



Mg (2.83 g, 116 mmol, 3.5 eq.) was placed in an oven-dried 500 mL three-neck round bottom flask equipped with a dropping funnel and a condenser and suspended in anhydrous diethyl ether (110 mL). 1-Bromo-3,5-bis(trifluoromethyl)benzene (25.95 g, 86.79 mmol, 2.6 eq.) was placed in the dropping funnel, dissolved in anhydrous diethyl ether (30 mL) and slowly added while stirring that the reaction mixture was kept at reflux. Afterward, the dark solution was refluxed for 2 h and cooled to 0 °C with an ice bath. (2S)-1,2-Pyrrolidinedicarboxylic acid 1-ethyl 2-methyl ester (6.72 g, 33.4 mmol, 1.0 eq.) was placed in the dropping funnel, dissolved in anhydrous diethyl ether (30 mL) and slowly added at 0 °C while stirring. After allowing the dark solution to warm up to room temperature, it was stirred for 16 h and saturated NH₄Cl (aq) was slowly added *via* the dropping funnel. After the phase separation, the organic phase was washed with brine, and the combined aqueous phases were extracted three times with chloroform (100 mL). The combined organic phases were dried over anhydrous MgSO₄, filtrated and evaporated. The red solid crude product was crystallized from methylcyclohexane.

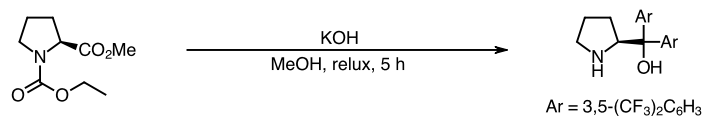
(2S)-2-[Bis[3,5-bis(trifluoromethyl)phenyl]hydroxymethyl]-1-pyrrolidinecarboxylic acid ethyl ester was obtained as a reddish solid (16.15 g, 27.03 mmol, 81%).

¹H NMR (400 MHz, CDCl₃) δ 7.89 (s, 1H), 7.86 (s, 3H), 7.82 (s, 2H), 7.00 (s, 1H), 4.86 (dd, *J* = 8.8, 5.3 Hz, 1H), 4.28 – 4.05 (m, 2H), 3.60 – 3.49 (m, 1H), 3.00 – 2.89 (m, 1H), 2.17 – 2.04 (m, 1H), 1.86 – 1.74 (m, 1H), 1.71 – 1.58 (m, 1H), 1.22 (t, *J* = 7.1 Hz, 3H), 1.08 – 0.95 (m, 1H).

¹³C NMR (101 MHz, CDCl₃) δ 158.94 (s), 147.27 (s), 145.26 (s), 131.95 (q), 131.56 (q), 128.13 (q), 127.74 (q), 124.66 (q), 122.43 – 121.91 (m), 80.90 (s), 66.84 (s), 62.91 (s), 48.12 (s), 30.35 (s), 23.37 (s), 14.59 (s).

Analytical data was in accordance with literature.⁵⁹

7.2.8 (2S)- α,α -Bis[3,5-bis(trifluoromethyl)phenyl]-2-pyrrolidinemethanol



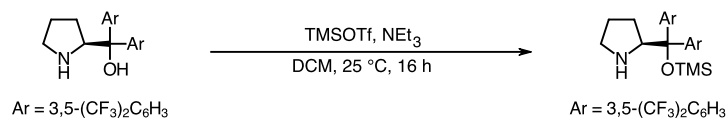
Ethyl (2S)-2-[bis[3,5-bis(trifluoromethyl)phenyl]hydroxymethyl]-1-pyrrolidinecarboxylic acid (16.15 g, 27.03 mmol, 1.0 eq.) was placed in a 1 L one-neck round bottle flask equipped with a condenser, dissolved in 2 M KOH in MeOH (450 mL) and the brown solution was refluxed for 5 h. The solvent was removed under vacuum and the brown solid residue was dissolved in distilled H₂O (200 mL) and DCM (100 mL). After the phase separation, the aqueous phase was extracted three times with DCM (100 mL) and the combined organic phases were washed with brine, dried over anhydrous MgSO₄, filtrated and evaporated.

(2S)- α,α -Bis[3,5-bis(trifluoromethyl)phenyl]-2-pyrrolidinemethanol was obtained as a brown solid (13.20 g, 25.12 mmol, 93%).

¹H NMR (400 MHz, CDCl₃) δ 8.04 (s, 2H), 7.96 (s, 2H), 7.77 (s, 1H), 7.76 (s, 1H), 5.06 (s, 1H), 4.35 (t, $J = 7.7$ Hz, 1H), 3.12 – 3.00 (m, 2H), 1.87 – 1.45 (m, 5H).

Analytical data was in accordance with literature.⁵⁹

7.2.9 (2S)-2-[Bis[3,5-bis(trifluoromethyl)phenyl][(trimethylsilyl)oxy]methyl]pyrrolidine (SA1)



(2S)- α,α -Bis[3,5-bis(trifluoromethyl)phenyl]-2-pyrrolidinemethanol (4.00 g, 7.61 mmol, 1.0 eq.) was placed in an oven-dried 250 mL three-neck round bottom flask equipped with a condenser and dissolved in anhydrous DCM (50 mL). NEt₃ (1.02 g, 9.90 mmol, 1.3 eq.) was added to the red solution at room temperature *via* syringe. After cooling the red solution to 0 °C with an ice bath, TMSOTf (2.25 g, 9.90 mmol, 1.3 eq.) was slowly added *via* syringe during vigorous stirring. The reaction mixture was allowed to warm up to room temperature and was stirred for 16 h. Afterward, distilled H₂O (50 mL) was added and after the phase separation, the aqueous phase was extracted three times with DCM (30 mL). The combined organic phases were dried over anhydrous MgSO₄, filtrated and evaporated. The red liquid crude product was purified *via* flash chromatography (silica, Et₂O:PE = 1:10, ninhydrin staining agent).

(2S)-2-[Bis[3,5-bis(trifluoromethyl)phenyl][(trimethylsilyl)oxy]methyl]pyrrolidine **SA1** was obtained as a yellow liquid (1.97 g, 3.30 mmol, 43%).

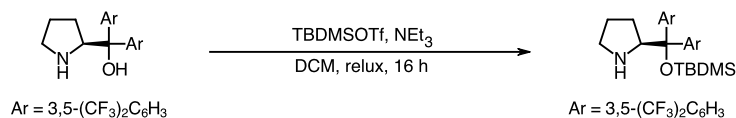
¹H NMR (600 MHz, CDCl₃) δ 8.00 (s, 2H), 7.84 (s, 1H), 7.83 (s, 1H), 7.76 (s, 2H), 4.22 (t, J = 7.4 Hz, 1H), 2.92 (dt, J = 10.3, 6.3 Hz, 1H), 2.56 (dt, J = 10.3, 6.7 Hz, 2H), 1.74 – 1.65 (m, 1H), 1.61 – 1.49 (m, 2H), 1.48 – 1.41 (m, 1H), 1.16 – 1.07 (m, 1H), -0.09 (s, 9H).

¹³C NMR (151 MHz, CDCl₃) δ 148.26 (s), 146.48 (s), 131.72 (q, J = 33.3 Hz), 130.97 (q, J = 33.2 Hz), 128.73 (d, J = 4.0 Hz), 128.20 (d, J = 3.8 Hz), 124.30 (d, J = 28.3 Hz), 122.49 (d, J = 28.6 Hz), 121.92 – 121.76 (m), 121.74 – 121.56 (m), 82.44 (s), 64.40 (s), 47.38 (s), 27.68 (s), 25.39 (s), 2.03 (s).

¹⁹F NMR (376 MHz, CDCl₃) δ -62.80 (s), -62.88 (s).

Analytical data was in accordance with literature.⁶⁰

7.2.10 (2S)-2-[Bis[3,5-bis(trifluoromethyl)phenyl]([(1,1-dimethylethyl)dimethylsilyl]oxy)methyl]pyrrolidine (SA2)



(2S)- α,α -Bis[3,5-bis(trifluoromethyl)phenyl]-2-pyrrolidinemethanol (4.00 g, 7.61 mmol, 1.0 eq.) was placed in an oven-dried 250 mL three-neck round bottom flask equipped with a condenser and dissolved in anhydrous DCM (50 mL). NEt₃ (4.72 g, 45.7 mmol, 6.0 eq.) was added to the red solution at room temperature *via* syringe. After cooling the red solution to 0 °C with an ice bath, TBDMSOTf (6.16 g, 22.8 mmol, 3.0 eq.) was slowly added *via* syringe during vigorous stirring. Afterward, the reaction mixture was refluxed for 16 h. Distilled H₂O (50 mL) was added at room temperature and after the phase separation, the aqueous phase was extracted three times with DCM (30 mL). The combined organic phases were dried over anhydrous MgSO₄, filtered and evaporated. The red liquid crude product was purified *via* flash chromatography (silica, Et₂O:PE = 1:20, ninhydrin staining agent).

(2S)-2-[Bis[3,5-bis(trifluoromethyl)phenyl]([(1,1-dimethylethyl)dimethylsilyl]oxy)methyl]pyrrolidine **SA2** was obtained as a yellow liquid (1.50 g, 2.34 mmol, 31%).

¹H NMR (600 MHz, CDCl₃) δ 8.09 (s, 2H), 7.85 (s, 2H), 7.74 (s, 2H), 4.27 – 4.23 (m, 1H), 2.93 – 2.87 (m, 1H), 2.53 (ddd, $J = 10.1, 6.9, 5.3$ Hz, 1H), 1.84 – 1.73 (m, 2H), 1.60 – 1.43 (m, 2H), 0.94 (s, 9H), 0.89 – 0.83 (m, 1H), -0.21 (s, 3H), -0.47 (s, 3H).

¹³C NMR (151 MHz, CDCl₃) δ 147.89 (s), 146.22 (s), 131.69 (q, $J = 33.3$ Hz), 130.74 (q, $J = 33.3$ Hz), 129.24 (d, $J = 3.8$ Hz), 128.88 (d, $J = 3.8$ Hz), 123.53 (q, $J = 272.7$ Hz), 123.28 (q, $J = 272.8$ Hz), 122.04 – 121.87 (m), 121.74 – 121.56 (m), 82.43 (s), 64.13 (s), 47.41 (s), 27.95 (s), 26.03 (s), 25.40 (s), 18.95 (s), -2.58 (s), -3.25 (s).

¹⁹F NMR (376 MHz, CDCl₃) δ -62.81 (s), -62.92 (s).

Analytical data was in accordance with literature.⁶¹

7.3 Asymmetric α -alkylation of ketones *via* direct enamine photoexcitation

7.3.1 Batch photoreactor set-up

All batch photoreactions were performed in a custom-made photoreactor composed of a cylindric case, lined out with 36 W LED stripes (365 nm) and placed on a magnetic stirrer to ensure stirring during the reaction (Figure 19). A beside-positioned fan ensured temperature control to maintain room temperature during the reaction. A matching perforated rack was placed on top of the photoreactor to ensure uniform irradiation of the Schlenk tubes (four simultaneously) at a distance of 2 cm from the light source.

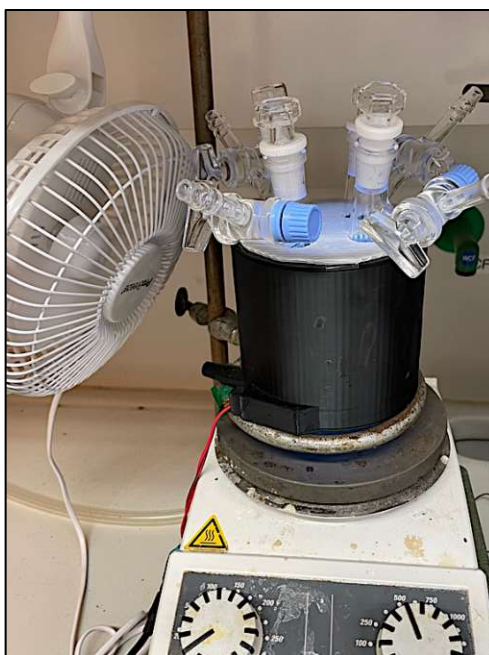


Figure 19: Batch photoreactor.

7.3.2 Flow photoreactor set-up

All continuous-flow photoreactions were performed in a Vaportec E-Series continuous-flow machine (Figure 20) equipped with a UV-150 photochemical reactor module and a dry-ice reliant integrated cooling system. The reactor module was composed of a

chamber in which a light-permeable fluorinated ethylene polymer (FEP) tubing (1 mm inside diameter, 10 mL) is coiled around a blue LED assembly (62 W, 365 nm).

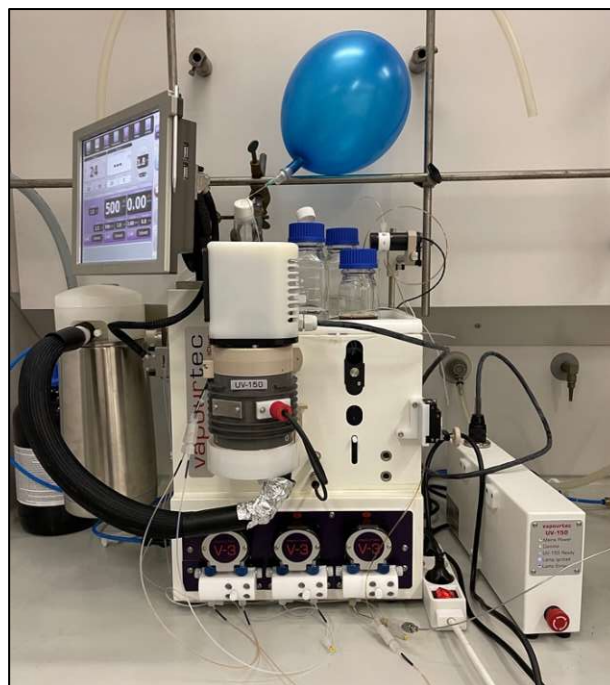


Figure 20: Flow photoreactor.

7.3.3 General considerations in batch

All batch photoreactions were carried out in Schlenk tubes (8 mL) and were prepared using the standard Schlenk technique. If the reaction mixture was homogeneous, it was separately prepared in a vial following the general procedure. The Schlenk tube was charged with the insoluble solid if the reaction mixture was heterogeneous. The remaining homogeneous reaction mixture was separately prepared in a vial following the general procedure. The Schlenk tube (empty or charged with solid) was evacuated and refilled with argon three times, and the separately prepared reaction mixture was added *via* syringe under argon counterflow. The Schlenk tube was sealed, placed into the custom-made photoreactor and the reaction mixture was stirred under irradiation for 16 h at room temperature.

7.3.4 General considerations in continuous-flow

All flow photoreactions were carried out in vials (10 mL) wrapped with parafilm and were prepared using the standard Schlenk technique. The reaction solution was prepared separately in a vial following the general procedure. The septum-closed vial was evacuated and refilled with argon three times *via* a syringe through the septum. The separately prepared reaction mixture was added *via* syringe through the septum under argon counterflow. The septum was pierced with a needle and the tube with the proper connection to the Vaportec E-Series continuous-flow machine was inserted above the solvent level. An argon-filled balloon equipped with a needle was inserted through the septum above the solvent level to ensure a positive argon pressure inside the vial when removing the vial from the Schlenk line. One end of the tube was connected to the pump system and the other was introduced into the reaction mixture. The tube system was conditioned with the used solvent for a couple of minutes, the temperature was set and the UV lamp was switched on before the reaction mixture was pumped at a certain flow rate through the photochemical reactor.

7.3.5 General procedure in batch

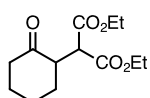
The catalyst (**Qn** · 2TFA, **Qd** · 2TFA or **PhQn**) (0.04 mmol, 0.2 eq.) was placed into a vial and dissolved in anhydrous solvent (0.2 M regarding the limiting component, 1 mL). To the solution, acid (0.08 mmol, 0.4 eq.), ketone **K** (0.80 mmol, 4.0 eq.) and alkyl halide **H** (0.20 mmol, 1.0 eq.) were added. If the preformed catalyst salt was used, the addition of acid was omitted. If the base (0.40 mmol, 2.0 eq.) was soluble, it was added to the vial. Otherwise, it was placed into the Schlenk tube. After evacuating and refilling the Schlenk tube with argon three times, the so pre-mixture was added *via* syringe under argon counterflow. The reaction mixture was stirred for 16 h under irradiation and at room temperature in the custom-made photoreactor. After completion, an aliquot (20 μ L) was taken for GCMS measurement. After the addition of EtOAc (2 mL), the suspension was filtrated through a Pasteur pipette filled with silica and washed three times with EtOAc (1 mL) to get rid of the catalyst, the base and the bromide salt (“crude work-up”). The solvent of the filtrate was removed under vacuum and the residue was dried under high vacuum. If the excess ketone **K** and the

unreacted alkyl halide **H** were sufficiently volatile, they could be distilled off, yielding the α -alkylated ketone **P** in satisfactory purity for chiral HPLC measurement.

To isolate the α -alkylated ketone **P**, two identical photoreaction samples were merged, the solvent was removed under vacuum and the residue was purified *via* flash chromatography.

7.3.6 Analytical data of α -alkylated ketones

7.3.6.1 1,3-Diethyl 2-(2-oxocyclohexyl)propanedioate (P1)



Prepared according to the general procedure using cyclohexanone **K1** (79.3 mg, 0.80 mmol, 4.0 eq.) and diethyl bromomalonate **H1** (48.8 mg, 0.20 mmol, 1.0 eq.). Purification by flash chromatography (silica, 10% EtOAc in PE, anisaldehyde staining agent) afforded **P1** as a colorless liquid.

Yield 65.9 mg (64%) using **Qn** · 2TFA

28.0 mg (27%) using **Qd** · 2TFA

ee 78% using **Qn** · 2TFA

72% using **Qd** · 2TFA

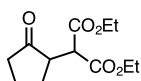
84% using **PhQn**

¹H NMR (400 MHz, CDCl₃) δ 4.25 – 4.13 (m, 4H), 3.65 (d, J = 9.5 Hz, 1H), 3.22 – 3.14 (m, 1H), 2.49 – 2.36 (m, 2H), 2.18 – 1.99 (m, 2H), 1.96 – 1.85 (m, 1H), 1.80 – 1.47 (m, 3H), 1.30 – 1.21 (m, 6H).

¹³C NMR (101 MHz, CDCl₃) δ 209.86 (s), 168.61 (d), 61.64 (s), 52.44 (s), 50.45 (s), 42.06 (s), 31.30 (s), 27.94 (s), 25.22 (s), 14.20 (d).

Analytical data was in accordance with literature.⁶²

7.3.6.2 1,3-Diethyl 2-(2-oxocyclopentyl)propanedioate (P2)



Prepared according to the general procedure using cyclopentanone **K2** (68.0 mg, 0.80 mmol, 4.0 eq.) and diethyl bromomalonate **H1** (48.8 mg, 0,20 mmol, 1.0 eq.). Purification by flash chromatography (silica, 20% EtOAc in PE, anisaldehyde staining agent) afforded **P2** as a colorless liquid.

Yield 20.7 mg (36%) using **Qn** · 2TFA

ee 54% using **Qn** · 2TFA

38% using **Qd** · 2TFA

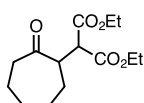
36% using **PhQn**

¹H NMR (400 MHz, CDCl₃) δ 4.26 – 4.06 (m, 4H), 3.74 (d, *J* = 5.6 Hz, 1H), 2.68 – 2.59 (m, 1H), 2.34 – 2.10 (m, 3H), 2.07 – 1.96 (m, 1H), 1.93 – 1.64 (m, 2H), 1.28 – 1.12 (m, 6H).

¹³C NMR (101 MHz, CDCl₃) δ 217.32 (s), 168.40 (d), 61.72 (s), 51.44 (s), 48.56 (s), 37.50 (s), 26.64 (s), 20.72 (s), 14.16 (d).

Analytical data was in accordance with literature.⁶²

7.3.6.3 1,3-Diethyl 2-(2-oxocycloheptyl)propanedioate (P3)



Prepared according to the general procedure using cycloheptanone **K3** (90.6 mg, 0.80 mmol, 4.0 eq.) and diethyl bromomalonate **H1** (48.8 mg, 0,20 mmol, 1.0 eq.). Purification by flash chromatography (silica, 5% EtOAc in PE, anisaldehyde staining agent) afforded **P3** as a colorless liquid.

Yield 13.1 mg (12%) using **Qn** · 2TFA

ee 40% using **Qn** · 2TFA

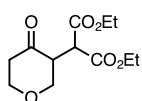
46% using **Qd** · 2TFA

30% using **PhQn**

¹H NMR (400 MHz, CDCl₃) δ 4.19 – 4.03 (m, 4H), 3.73 (d, *J* = 10.2 Hz, 1H), 3.38 – 3.31 (m, 1H), 2.67 – 2.58 (m, 1H), 2.44 – 2.33 (m, 1H), 1.91 – 1.24 (m, 8H), 1.24 – 1.13 (m, 6H).

¹³C NMR (101 MHz, CDCl₃) δ 213.12 (s), 168.82 (d), 61.70 (d), 54.33 (s), 50.45 (s), 43.59 (s), 29.55 (s), 29.03 (s), 28.48 (s), 23.14 (s), 14.19 (d).

7.3.6.4 1,3-Diethyl 2-(tetrahydro-4-oxo-2*H*-pyran-3-yl)propanedioate (**P4**)



Prepared according to the general procedure using tetrahydro-4*H*-pyran-4-one **K4** (80.9 mg, 0.80 mmol, 4.0 eq.) and diethyl bromomalonate **H1** (48.8 mg, 0.20 mmol, 1.0 eq.). Purification by flash chromatography (silica, 10% EtOAc in PE, anisaldehyde staining agent) afforded **P4** as a colorless liquid.

Yield 53.2 mg (51%) using **Qn** · 2TFA

ee 8% using **Qn** · 2TFA

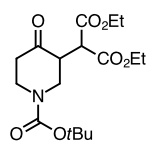
36% using **Qd** · 2TFA

82% using **PhQn**

¹H NMR (400 MHz, CDCl₃) δ 4.26 – 4.08 (m, 6H), 3.69 – 3.58 (m, 3H), 3.33 – 3.25 (m, 1H), 2.72 – 2.61 (m, 1H), 2.41 – 2.33 (m, 1H), 1.24 – 1.16 (m, 6H).

¹³C NMR (101 MHz, CDCl₃) δ 205.07 (s), 167.83 (d), 70.24 (s), 68.50 (s), 61.92 (d), 50.53 (s), 49.05 (s), 42.57 (s), 14.11 (d).

7.3.6.5 1-(1,1-Dimethylethyl) 3,3-diethyl 4-oxo-1,3,3-piperidinetricarboxylate (P5)



Prepared according to the general procedure using *tert*-butyl 4-oxopiperidine-1-carboxylate **K5** (159.4 mg, 0.80 mmol, 4.0 eq.) and diethyl bromomalonate **H1** (48.8 mg, 0.20 mmol, 1.0 eq.). Purification by flash chromatography (silica, 8% EtOAc in PE, anisaldehyde staining agent) afforded a mixture of **P5** and **K5** as a white solid. The yield was calculated from GC peak areas, the ¹H NMR contained substrate and the enantiomers were identified from their UV absorption spectra.

Yield 19.1 mg (24%) using **Qn** · 2TFA

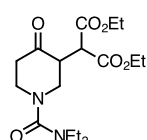
ee 18% using **Qn** · 2TFA

4% using **Qd** · 2TFA

70% using **PhQn**

¹H NMR (400 MHz, CDCl₃) δ 4.42 – 4.16 (m, 6H), 3.99 – 3.92 (m, 1H), 3.22 – 3.06 (m, 3H), 2.62 – 2.50 (m, 2H), 1.48 (s, 9H), 1.31 – 1.23 (m, 6H).

7.3.6.6 3,3-Diethyl 1-[(diethylamino)carbonyl]-4-oxo-3-piperidinedicarboxylate (P6)



Prepared according to the general procedure using *N,N*-diethyl-4-oxo-1-piperidinecarboxamide **K6** (158.6 mg, 0.80 mmol, 4.0 eq.) and diethyl bromomalonate **H1** (48.8 mg, 0.20 mmol, 1.0 eq.). Purification by flash chromatography (silica, 30% EtOAc in PE, anisaldehyde staining agent) afforded a mixture of **P6** and **K6** as a yellow liquid. The yield was calculated from GC peak areas, the ¹H NMR contained substrate and the enantiomers were identified from their UV absorption spectra.

Yield 28.8 mg (36%) using **Qn** · 2TFA

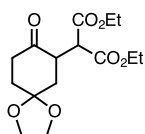
ee 64% using **Qn** · 2TFA

96% using **Qd** · 2TFA

92% using **PhQn**

¹H NMR (400 MHz, CDCl₃) δ 4.14 (q, *J* = 7.1 Hz, 4H), 3.90 – 3.76 (m, 2H), 3.68 (d, *J* = 7.9 Hz, 1H), 3.20 (q, *J* = 7.1, 4H), 3.13 – 2.99 (m, 3H), 2.69 – 2.58 (m, 1H), 2.39 – 2.33 (m, 1H), 1.21 (t, *J* = 7.1, 6H), 1.09 (t, *J* = 7.1, 6H).

7.3.6.7 1,3-Diethyl 2-(8-oxo-1,4-dioxaspiro[4.5]dec-7-yl)propanedioate (**P7**)



Prepared according to the general procedure using 1,4-dioxaspiro[4.5]decan-8-one **K8** (126.2 mg, 0.80 mmol, 4.0 eq.) and diethyl bromomalonate **H1** (48.8 mg, 0.20 mmol, 1.0 eq.). Purification by flash chromatography (silica, 15% EtOAc in PE, anisaldehyde staining agent) afforded a mixture of **P7** as a colorless liquid.

Yield 68.0 mg (54%) using **Qn** · 2TFA

ee 66% using **Qn** · 2TFA

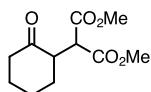
76% using **Qd** · 2TFA

86% using **PhQn**

¹H NMR (400 MHz, CDCl₃) δ 4.24 – 4.11 (m, 4H), 4.06 – 3.95 (m, 4H), 3.68 (d, *J* = 8.5 Hz, 1H), 3.53 – 3.42 (m, 1H), 2.79 – 2.65 (m, 1H), 2.43 – 2.35 (m, 1H), 2.09 – 1.91 (m, 4H), 1.28 – 1.29 (m, 6H).

¹³C NMR (101 MHz, CDCl₃) δ 208.28 (s), 168.24 (s), 107.11 (s), 64.83 (d), 61.63 (d), 51.61 (s), 46.42 (s), 37.86 (s), 37.53 (s), 34.52 (s), 14.14 (d).

7.3.6.8 1,3-Dimethyl 2-(2-oxocyclohexyl)propanedioate (P8)



Prepared according to the general procedure using cyclohexanone **K1** (79.3 mg, 0.80 mmol, 4.0 eq.) and dimethyl bromomalonate **H2** (42.2 mg, 0.20 mmol, 1.0 eq.). Purification by flash chromatography (silica, 10% EtOAc in PE, anisaldehyde staining agent) afforded a mixture of **P8** as a colorless liquid.

Yield 45.7 mg (50%) using **Qn** · 2TFA

ee 51% using **Qn** · 2TFA

45% using **Qd** · 2TFA

80% using **PhQn**

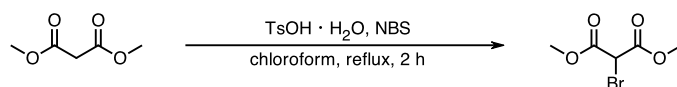
¹H NMR (400 MHz, CDCl₃) δ 3.72 (d, *J* = 1.8 Hz, 6H), 3.67 (d, *J* = 9.5 Hz, 1H), 3.23 – 3.14 (m, 1H), 2.46 – 2.34 (m, 2H), 2.15 – 2.07 (m, 1H), 2.06 – 1.98 (m, 1H), 1.94 – 1.86 (m, 1H), 1.77 – 1.47 (m, 3H).

¹³C NMR (101 MHz, CDCl₃) δ 209.76 (s), 168.97 (d), 52.76 (d), 52.06 (s), 50.53 (s), 41.99 (s), 31.33 (s), 27.87 (s), 25.15 (s).

Analytical data was in accordance with literature.⁶³

7.4 Substrate synthesis

7.4.1 1,3-Dimethyl 2-bromopropanedioate (H2)



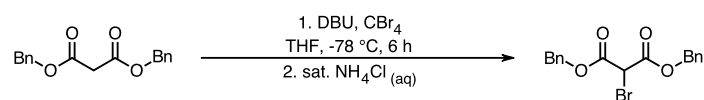
Dimethyl malonate (2.64 g, 20.0 mmol, 1.0 eq.) was placed in a 100 mL one-neck round bottom flask equipped with a condenser and dissolved in DCM (30 mL). TsOH · H₂O (0.78 g, 4.0 mmol, 0.2 eq.) and NBS (3.60 g, 20.0 mmol, 1.0 eq.) were added and the yellow solution was refluxed for 2 h. The solvent was removed under vacuum and the solid residue was suspended in diethyl ether (30 mL). After filtration, distilled H₂O (30 mL) was added to the filtrate and the phases were separated. The aqueous phase was extracted three times with diethyl ether (20 mL), and the combined organic phases were dried over anhydrous MgSO₄, filtrated and evaporated. The yellow liquid crude product was purified *via* distillation (115 °C at 25 mbar).

1,3-Dimethyl 2-bromopropanedioate **H2** was obtained as a colorless liquid (2.46 g, 11.7 mmol, 58%).

¹H NMR (400 MHz, CDCl₃) δ 4.86 (s, 1H), 3.84 (s, 6H).

Analytical data was in accordance with literature.⁶⁴

7.4.2 1,3-Bis(phenylmethyl) 2-bromopropanedioate (H4)



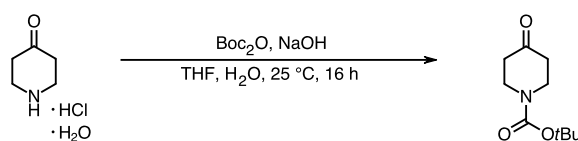
Dibenzyl malonate (3.67 g, 12.3 mmol, 1.0 eq.) was placed in a 250 mL three-neck round bottom flask equipped with a condenser and dissolved in anhydrous THF (100 mL). The colorless solution was cooled to 0 °C with an ice bath and DBU (1.88 g, 12.3 mmol, 1.0 eq.) was slowly added *via* syringe. The colorless solution was cooled to -78 °C with an acetone/ dry ice bath, CBr₄ (4.10 g, 12.3 mmol, 1.0 eq.) was added and the yellow solution was stirred at -78 °C for 6 h. Saturated NH₄Cl (aq) (50 mL) and distilled H₂O (10 mL) were added. The yellow reactions mixture was allowed to warm up to room temperature. After the phase separation, the organic phase was washed with brine and the combined aqueous phases were extracted three times with DCM (20 mL). The combined organic phases were dried over anhydrous MgSO₄, filtrated and evaporated. The yellow liquid crude product was purified *via* flash chromatography (silica, EtOAc:PE = 1:20, vanillin staining agent).

1,3-Bis(phenylmethyl) 2-bromopropanedioate **H4** was obtained as a colorless liquid (1.17 g, 3.22 mmol, 26%).

¹H NMR (400 MHz, CDCl₃) δ 7.37 – 7.28 (m, 10H), 5.22 (s, 4H), 4.92 (s, 1H).

Analytical data was in accordance with literature.⁶⁵

7.4.3 *tert*-Butyl 4-oxopiperidine-1-carboxylate (K5)



4-Piperidone monohydrate hydrochloride (3.14 g, 20.0 mmol, 1.0 eq.) was placed in a 100 mL three-neck round bottom flask equipped with a dropping funnel and a condenser and dissolved in distilled H_2O (25 mL) and THF (25 mL). NaOH (0.80 g, 20.0 mmol, 1.0 eq.) was added to the biphasic system. Boc_2O (5.29 g, 24.0 mmol, 1.2 eq.) was placed in the dropping funnel, dissolved in THF (20 mL) and added to the biphasic system. The reaction mixture was stirred at room temperature for 16 h. After the evaporation of THF, EtOAc (40 mL) was added and the phases were separated. The aqueous phase was extracted with EtOAc (20 mL) three times, and the combined organic phases were dried over anhydrous MgSO_4 , filtrated and evaporated. The yellow solid crude product was recrystallized from *n*-heptane (20 mL).

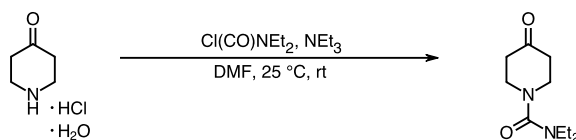
tert-Butyl 4-oxopiperidine-1-carboxylate **K5** was obtained as a white solid (1.86 g, 9.34 mmol, 47%).

$^1\text{H NMR}$ (400 MHz, CDCl_3) δ 3.71 (t, $J = 6.2$ Hz, 4H), 2.43 (t, $J = 6.2$ Hz, 4H), 1.49 (s, 4H).

$^{13}\text{C NMR}$ (101 MHz, CDCl_3) δ 207.96 (s), 154.62 (s), 80.59 (s), 41.32 (s), 28.51 (s).

Analytical data was in accordance with literature.⁶⁶

7.4.4 *N,N*-Diethyl-4-oxo-1-piperidinecarboxamide (K6)



4-Piperidone monohydrate hydrochloride (3.14 g, 20.0 mmol, 1.0 eq.) was placed in a 100 mL three-neck round bottom flask equipped with a condenser and suspended in anhydrous DMF (40 mL). After the addition of NEt₃ (6.07 g, 60.0 mmol, 3.0 eq.), diethylcarbamoyl chloride (4.19 g, 30.0 mmol, 1.5 eq.) was slowly added *via* syringe during vigorous stirring. The yellow reaction mixture was stirred at room temperature for 16 h. The solvent was removed under vacuum. The yellow solid residue was dissolved in EtOAc (40 mL) and distilled H₂O (40 mL). After the phase separation, the aqueous phase was extracted with EtOAc three times and the combined organic phases were washed with brine, dried over MgSO₄, filtrated and evaporated. The yellow liquid crude product was purified *via* flash chromatography (silica, MeOH:DCM = 1:100, anisaldehyde staining agent).

N,N-Diethyl-4-oxo-1-piperidinecarboxamide **K6** was obtained as a yellow liquid (2.45 g, 12.3 mmol, 62%).

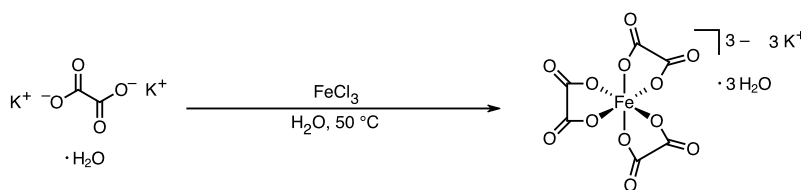
¹H NMR (400 MHz, CDCl₃) δ 3.49 (t, *J* = 6.2 Hz, 4H), 3.26 (q, *J* = 7.1 Hz, 4H), 2.48 (t, *J* = 6.1 Hz, 4H), 1.15 (t, *J* = 7.1 Hz, 6H).

7.5 Quantum yield determination

The photon flux of the custom-made photoreactor was determined using the ferrioxalate actinometer according to the Hammond variation of the Hatchard and Parker procedure⁶⁷ described in the Handbook of Photochemistry.⁶⁸

Potassium ferrioxalate $K_3[Fe(C_2O_4)_3]$ is a photolabile complex that reductively decomposes upon irradiation under the formation of ferrous iron (Fe^{2+}), that is complexed by 1,10-phenanthroline. The formation of the colored ferrioxalate ($[Fe(1,10-phen)_3]SO_4$) can be monitored *via* UV/Vis spectroscopy at 510 nm to measure the ratio of ferric (Fe^{3+}) to ferrous iron. The moles of formed ferrioxalate are proportional to the moles of absorbed photons, and the quantum yield of potassium ferrioxalate depends on the concentration and irradiation wavelength.

7.5.1 Synthesis of potassium ferrioxalate



Potassium oxalate monohydrate (2.97 g, 16.1 mmol, 3.0 eq.) was placed in a vial and dissolved in distilled H_2O (9 mL). A solution of $FeCl_3$ (0.87 g, 5.38 mmol, 1.0 eq.) dissolved in distilled H_2O (2.5 mL) was added *via* syringe at 50 °C while stirring. The green solution was cooled to 0 °C for 16 h. The green crystals were filtrated, washed with distilled H_2O , dried and stored in the dark.

Potassium ferrioxalate trihydrate was obtained as a green crystalline solid (1.84 g, 3.75 mmol, 70 %).

FT-IR (ATR, cm^{-1}) 3431 (ν_{OH}), 1689 (ν_{CO}), 1380, 1256, 891, 787.

Analytical data was in accordance with literature.⁶⁹

7.5.2 Determination of the photon flux

Potassium ferrioxalate solution: Potassium ferrioxalate trihydrate (147.4 mg, 0.30 mmol) and concentrated sulfuric acid (69.5 μL) were placed in a 25 mL volumetric flask and filled up with distilled H_2O .

1,10-Phenanthroline solution: 1,10-Phenanthroline (100.0 mg, 0.55 mmol) was placed in a 50 mL volumetric flask and filled with distilled H_2O .

Buffer solution: NaOAc (4.94 g, 60.2 mmol) and concentrated sulfuric acid (1 mL) were placed in a 100 mL volumetric flask and filled up with distilled H_2O .

Four 8 mL Schlenk tubes were charged with Potassium ferrioxalate solution (1 mL), placed in the custom-made photoreactor, and irradiated in sequence for 3 s, 5 s, 10 s and 15 s while stirring. Afterward, each irradiated sample and a non-irradiated sample (0 s) were transferred into a 10 mL volumetric flask, 1,10-phenanthroline solution (0.5 mL) and buffer solution (2.0 mL) were added and filled up with distilled H_2O . The samples were wrapped in aluminum foil to avoid light exposure. After a 1 h waiting period at room temperature, they were analyzed by UV/Vis spectroscopy (Figure 21).

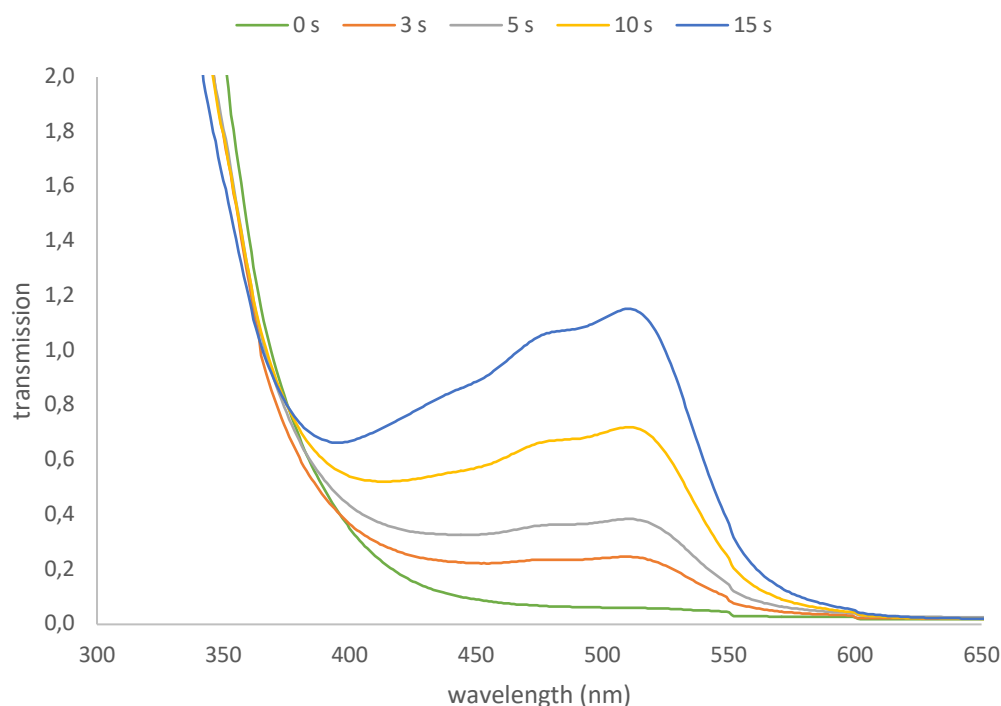


Figure 21: UV/Vis spectra of the photon flux determination samples after certain irradiation times.

The moles of formed ferrous iron in each sample was calculated with the Lambert-Beer equation (eq. 2).

$$n(\text{Fe}^{2+}) = \frac{V_1 \cdot V_3 \cdot \Delta A(510 \text{ nm})}{10^3 \cdot V_2 \cdot l \cdot \epsilon(510 \text{ nm})} \quad (\text{eq. 2})$$

$n(\text{Fe}^{2+})$... amount of substance of ferrous iron (mol)
V_1	... irradiated volume (1 mL)
V_2	... aliquot of the irradiated solution for the determination of the ferrous iron (1 mL)
V_3	... final volume (10 mL)
l	... optical path length (1 cm)
$\Delta A(510 \text{ nm})$... absorption difference of the irradiated and the non-irradiated sample at 510 nm
$\epsilon(510 \text{ nm})$... extinction coefficient of ferriox at 510 nm (11100 L mol ⁻¹ cm ⁻¹)

The amount of substance of ferrous iron is plotted as a function of time (Figure 22). The slope of this straight line is used to determine the moles of incident photons by the unit of time by the custom-made photoreactor (eq. 3). To determine the ratio of absorbed photons by the solution, a non-irradiated and non-complexed sample was analyzed by UV/Vis spectroscopy. Therefore, potassium ferrioxalate solution (1 mL) was placed in a 10 mL volumetric flask, buffer solution (2 mL) was added and filled with distilled H₂O.

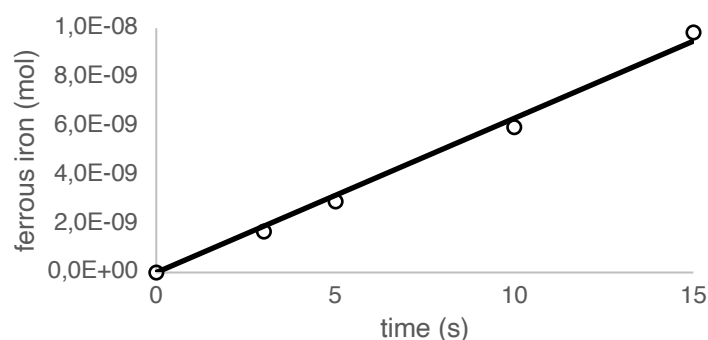


Figure 22: Moles of formed ferrous iron versus the irradiation time. $y = 6.31\text{E-}08x$, $R^2 = 9.97\text{E-}01$.

$$\text{photon flux} = \frac{\text{slope}_{\text{actinometer}}}{\Phi_{\text{actinometer}}(\lambda) \cdot [1 - 10^{-A_{\text{actinometer}}(\lambda)}]} \quad (\text{eq. 3})$$

photon flux ... photon flux of the custom-made photoreactor (Einstein s⁻¹)

slope_{actinometer} ... moles of formed ferrous ions by the unit of time (mol s⁻¹)

Φ_{actinometer}(λ) ... quantum yield of potassium ferrioxalate at 365 nm (1.27)⁷⁰

A_{actinometer}(λ) ... absorption of the non-irradiated and non-complexed sample at 365 nm (1.054)

The photon flux of the custom-made photoreactor was calculated as **5.45 × 10⁻⁸ Einstein s⁻¹**.

7.5.3 Determination of the quantum yield

Standard solution: Ethyl benzoate (330.0 mg, 2.20 mmol) was placed in a 5 mL volumetric flask and filled with DCM.

The model reaction mixture was prepared four times in four vials, each by dissolving **Qn** · 2TFA (22.06 mg, 0.04 mmol, 0.2 eq.) in anhydrous DCM (1 mL) and adding cyclohexanone (67.98 mg, 0.80 mmol, 4.0 eq.), diethyl bromomalonate (48.79 mg, 0.20 mmol, 1.0 eq.) and 2,6-lutidine (43.30 mg, 0.40 mmol, 2.0 eq.). After evacuating and refilling with argon for three times, each model reaction mixture was transferred into an 8 mL Schlenk tube in argon counterflow. The sealed samples were placed in the custom-made photoreactor and irradiated in a sequence for 10 min, 20 min, 30 min and 40 min while stirring. Afterward, standard solution (150 μL) was added to each sample and the yield was determined from an aliquot *via* GC-FID analysis.

The amount of substance of the product is plotted against the number of absorbed photons (Figure 23). The slope of this straight line is used for the determination of the quantum yield of the reaction (eq. 3). To determine the ratio of absorbed photons by the solution, a catalyst-free sample was analyzed by UV/Vis spectroscopy. Therefore, TFA (9.21 mg, 0.08 mmol, 0.4 eq.), cyclohexanone (67.98 mg, 0.80 mmol, 4.0 eq.), diethyl bromomalonate (48.79 mg, 0.20 mmol, 1.0 eq.) and 2,6-lutidine (43.30 mg, 0.40 mmol, 2.0 eq.) were placed in a vial and dissolved in anhydrous DCM (1 mL).

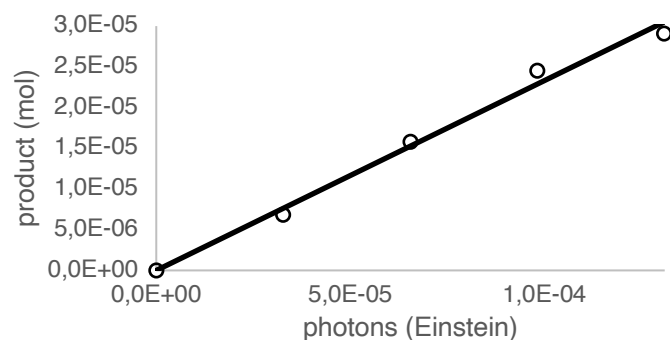


Figure 23: Moles of formed product versus the number of absorbed photons. $y = 2.33E-01x$, $R^2 = 9.97E-01$.

$$\Phi_{\text{reaction}}(\lambda) = \frac{\text{slope}_{\text{reaction}}}{[1 - 10^{-A_{\text{reaction}}(\lambda)}]} \quad (\text{eq. 4})$$

Φ_{reaction} ... quantum yield of the reaction at 365 nm

$\text{slope}_{\text{reaction}}$... moles of the formed product by the unit of absorbed photons

$A_{\text{reaction}}(\lambda)$... absorption of the catalyst-free sample at 365 nm (0.199)

The quantum yield of the model reaction was calculated as **0.63**.

8 References

1. V. Sojo, *Origins of Life and Evolution of Biospheres*, 2015, **45**, 219-224.
2. D. Voet, J. G. Voet and C. W. Pratt, *Lehrbuch der Biochemie*, John Wiley & Sons, 2019.
3. A. Matlack, *Introduction to green chemistry*, CRC press, 2010.
4. S. Zhu and D. Wang, *Advanced Energy Materials*, 2017, **7**, 1700841.
5. P. Y. Bruice, *Organische Chemie: Studieren kompakt*, Pearson Deutschland GmbH, 2011.
6. I. Fleming, *Molecular orbitals and organic chemical reactions*, John Wiley & Sons, 2011.
7. R. Cano, A. Zakarian and G. P. McGlacken, *Angewandte Chemie International Edition*, 2017, **56**, 9278-9290.
8. G. Wedler and H.-J. Freund, *Lehrbuch der physikalischen Chemie*, John Wiley & Sons, 2012.
9. J. García-Álvarez, *Molecules*, 2020, **25**, 1493.
10. B. Han, X.-H. He, Y.-Q. Liu, G. He, C. Peng and J.-L. Li, *Chemical Society Reviews*, 2021, **50**, 1522-1586.
11. W. Yao, E. A. Bazan-Bergamino and M.-Y. Ngai, *ChemCatChem*, 2022, **14**, e202101292.
12. D. M. Arias-Rotondo and J. K. McCusker, *Chemical Society Reviews*, 2016, **45**, 5803-5820.
13. N. A. Romero and D. A. Nicewicz, *Chemical Reviews*, 2016, **116**, 10075-10166.
14. R. R. Knowles and E. N. Jacobsen, *Proceedings of the National Academy of Sciences*, 2010, **107**, 20678-20685.
15. D. M. Hodgson and A. Charlton, *Tetrahedron*, 2014, **70**, 2207-2236.
16. P. Melchiorre, *Angewandte Chemie International Edition*, 2012, **51**, 9748-9770.
17. S. Mukherjee, J. W. Yang, S. Hoffmann and B. List, *Chemical Reviews*, 2007, **107**, 5471-5569.
18. B. Matos Paz, H. Jiang and K. A. Jørgensen, *Chemistry – A European Journal*, 2015, **21**, 1846-1853.
19. T. B. Wright and P. A. Evans, *Chemical Reviews*, 2021, **121**, 9196-9242.
20. A. Job, C. F. Janeck, W. Bettray, R. Peters and D. Enders, *Tetrahedron*, 2002, **58**, 2253-2329.
21. Y. Gnas and F. Glorius, *Synthesis*, 2006, **2006**, 1899-1930.
22. M. Oiarbide and C. Palomo, *Chemistry – A European Journal*, 2021, **27**, 10226-10246.
23. B. M. Trost, G. M. Schroeder and J. Kristensen, *Angewandte Chemie*, 2002, **114**, 3642-3645.
24. G. Jiang and B. List, *Angewandte Chemie International Edition*, 2011, **50**, 9471-9474.
25. S. Afewerki, I. Ibrahim, J. Rydfjord, P. Breistein and A. Córdova, *Chemistry – A European Journal*, 2012, **18**, 2972-2977.
26. S. Krautwald, D. Sarlah, M. A. Schafroth and E. M. Carreira, *Science*, 2013, **340**, 1065-1068.
27. H.-E. Lee, D. Kim, A. You, M. H. Park, M. Kim and C. Kim, *Catalysts*, 2020, **10**, 861.
28. A. E. Nibbs, A.-L. Baize, R. M. Herter and K. A. Scheidt, *Org. Lett.*, 2009, **11**, 4010-4013.
29. N. Vignola and B. List, *Journal of the American Chemical Society*, 2004, **126**, 450-451.
30. P. G. Cozzi, F. Benfatti and L. Zoli, *Angewandte Chemie International Edition*, 2009, **48**, 1313-1316.
31. M. Guiteras Capdevila, E. Emer, F. Benfatti, A. Gualandi, C. M. Wilson and P. G. Cozzi, *Asian Journal of Organic Chemistry*, 2012, **1**, 38-42.

32. A. R. Brown, W.-H. Kuo and E. N. Jacobsen, *Journal of the American Chemical Society*, 2010, **132**, 9286-9288.
33. T. D. Beeson, A. Mastracchio, J.-B. Hong, K. Ashton and D. W. C. MacMillan, *Science*, 2007, **316**, 582-585.
34. M. Mečiarová, P. Tisovský and R. Šebesta, *New Journal of Chemistry*, 2016, **40**, 4855-4864.
35. K. Zeitler and M. Neumann, *Physical Sciences Reviews*, 2020, **5**.
36. D. A. Nicewicz and D. W. C. MacMillan, *Science*, 2008, **322**, 77-80.
37. M. Neumann, S. Földner, B. König and K. Zeitler, *Angewandte Chemie International Edition*, 2011, **50**, 951-954.
38. P. Wu, C. He, J. Wang, X. Peng, X. Li, Y. An and C. Duan, *Journal of the American Chemical Society*, 2012, **134**, 14991-14999.
39. Y. Zhu, L. Zhang and S. Luo, *Journal of the American Chemical Society*, 2014, **136**, 14642-14645.
40. E. Arceo, I. D. Jurberg, A. Álvarez-Fernández and P. Melchiorre, *Nature Chemistry*, 2013, **5**, 750-756.
41. E. Arceo, A. Bahamonde, G. Bergonzini and P. Melchiorre, *Chemical Science*, 2014, **5**, 2438-2442.
42. C. G. S. Lima, T. de M. Lima, M. Duarte, I. D. Jurberg and M. W. Paixão, *ACS Catalysis*, 2016, **6**, 1389-1407.
43. M. Silvi, E. Arceo, I. D. Jurberg, C. Cassani and P. Melchiorre, *Journal of the American Chemical Society*, 2015, **137**, 6120-6123.
44. A.-N. Alba, M. Viciano and R. Rios, *ChemCatChem*, 2009, **1**, 437-439.
45. C. Cassani, R. Martín-Rapún, E. Arceo, F. Bravo and P. Melchiorre, *Nature Protocols*, 2013, **8**, 325-344.
46. T. E. Schirmer and B. König, *Journal of the American Chemical Society*, 2022, **144**, 19207-19218.
47. K. Nakajima, Y. Miyake and Y. Nishibayashi, *Accounts of Chemical Research*, 2016, **49**, 1946-1956.
48. T. A. B. M. Bolsman, A. P. Blok and J. H. G. Frijns, *Recueil des Travaux Chimiques des Pays-Bas*, 1978, **97**, 313-319.
49. A. Eibel, D. E. Fast and G. Gescheidt, *Polymer Chemistry*, 2018, **9**, 5107-5115.
50. L. Buzzetti, G. E. M. Crisenza and P. Melchiorre, *Angewandte Chemie International Edition*, 2019, **58**, 3730-3747.
51. I. R. Baxendale, *Journal of Chemical Technology & Biotechnology*, 2013, **88**, 519-552.
52. K. Donnelly and M. Baumann, *Journal of Flow Chemistry*, 2021, **11**, 223-241.
53. M. Di Filippo, C. Bracken and M. Baumann, *Molecules*, 2020, **25**, 356.
54. F. Scharinger, Á. M. Pálvölgyi, M. Weisz, M. Weil, C. Stanetty, M. Schnürch and K. Bica-Schröder, *Angewandte Chemie International Edition*, 2022, **61**, e202202189.
55. F. Scharinger, Á. Márk Pálvölgyi, V. Zeindlhofer, M. Schnürch, C. Schröder and K. Bica-Schröder, *ChemCatChem*, 2020, **12**, 3776-3782.
56. G. Varró, L. Hegedűs, A. Simon, A. Balogh, A. Grün, I. Leveles, B. G. Vértessy and I. Kádas, *Journal of Natural Products*, 2017, **80**, 1909-1917.
57. I. D. Jurberg, *Chemistry – A European Journal*, 2017, **23**, 9716-9720.
58. F.-M. Gautier, S. Jones and S. J. Martin, *Organic & Biomolecular Chemistry*, 2009, **7**, 229-231.

59. Z. Dalicsek, F. Pollreisz and T. Soós, *Chemical Communications*, 2009, DOI: 10.1039/B908967E, 4587-4589.
60. M. Marigo, T. C. Wabnitz, D. Fielenbach and K. A. Jørgensen, *Angewandte Chemie International Edition*, 2005, **44**, 794-797.
61. M. L. J. Wong, A. J. Sterling, J. J. Mousseau, F. Duarte and E. A. Anderson, *Nature Communications*, 2021, **12**, 1644.
62. E. Fuks, L. Huber, T. Schinkel and O. Trapp, *European Journal of Organic Chemistry*, 2020, **2020**, 6192-6198.
63. N. Esumi, K. Suzuki, Y. Nishimoto and M. Yasuda, *Org. Lett.*, 2016, **18**, 5704-5707.
64. S. Adimurthy, G. Ramachandraiah, A. V. Bedekar, S. Ghosh, B. C. Ranu and P. K. Ghosh, *Green Chemistry*, 2006, **8**, 916-922.
65. L. B. Marx and J. W. Burton, *Chemistry – A European Journal*, 2018, **24**, 6747-6754.
66. B. Peschke, M. Ankersen, B. Sehested Hansen, T. Kruse Hansen, N. Langeland Johansen, J. Lau, K. Madsen, H. Petersen, H. Thøgersen and B. Watson, *European Journal of Medicinal Chemistry*, 1999, **34**, 363-380.
67. C. G. Hatchard, C. A. Parker and E. J. Bowen, *Proceedings of the Royal Society of London. Series A. Mathematical and Physical Sciences*, 1956, **235**, 518-536.
68. M. Montalti, L. Prodi, M. T. Gandolfi, *Handbook of Photochemistry (3rd ed.)*, CRC press, 2006.
69. J. Carriazo, *Chemistry*, 2010, **19**, 103-112.
70. J. Rabani, H. Mamane, D. Pousty and J. R. Bolton, *Photochemistry and Photobiology*, 2021, **97**, 873-902.